Prog. Oceanog. Vol. 26, pp. 263-306, 1991.
Printed in Great Britain.

0079-6611/91 $0.00 + .50

Light and marine photosynthesis: a spectral model with geochemical and climatological implications

ANDRÉ MOREL

Laboratoire de Physique et Chimie Marines, Université Pierre et Marie Curie, BP 8, F 06230 Villefranche sur Mer, France

(*Submitted 2 December 1988; Accepted in revised form November 1989*)

Abstract - Recent studies by MOREL (1978) and PLATT, SATHYENDRANATH, CAVERHILL and LEWIS (1988) have demonstrated the relative stability of the relationship between available photosynthetic energy at the ocean surface and energy stored by algal photosynthesis, once it has been normalized with respect to the column integrated chlorophyll biomass.

Therefore the cross section vis a vis photosynthesis and per unit of areal chlorophyll, ψ^*, in m^2 (g Chl)$^{-1}$, should be relatively stable in spite of the various environmental and trophic situations possibly encountered in the open ocean. Such an ecological or biogeochemical "constant" is of importance when trying to transform biomass maps (obtained from remotely sensed ocean colour data) into primary production maps. Its approximate constancy has to be understood and deserves analysis.

This analysis rests on the use of the local and instantaneous growth rate equation (KIEFER and MITCHELL, 1983) which has to be triply integrated with respect to wavelength, depth and time. Such an integration is, in effect, the core of a light production model which schematically includes the following steps:

(i) to compute as a function of the sun elevation for various days, latitudes and atmospheric conditions (aerosols, water vapour, etc.) the photosynthetic energy impinging at the ocean surface (direct and diffuse components);

(ii) to account for the loss by reflection at the air-sea interface;

(iii) to propagate this radiant energy (in terms of spectral scalar irradiance) throughout the water column and according to given pigment vertical profiles;

(iv) to evaluate what part of energy is absorbed by algae within the productive column;

(v) and finally to compute that part of absorbed energy which is stored in the form of organic carbon added to the initial biomass; this last step implies that the yield for growth be modelled as a function of the irradiance level and temperature.

Sensitivity tests have been effected with respect not only to the physical parameters which can be accurately modelled, but also with respect to the physiological factors for which values and parameterisation are more uncertain. Non-linear and interactive influences cause the ψ^* values obtained by running the model, to vary within a rather restricted range (within a factor 2, for most of the trophic and environmental conditions), which are similar to those resulting from field studies. The variability of the biomass-normalized primary production can be explained and the seasonal or zonal trends illustrated. The effect of cloudiness is also analysed. This spectral light – photosynthesis model (a sub model in the more general study of the biomass evolution) can be used either to reproduce primary production experiments and also as a predictive tool in the oceanic carbon fixation problem. The global scale made accessible by satellite techniques requires that a climatological field of the ψ^* parameter be produced. This can be done by operating the present model, provided that the physiological factors which intervene are sufficiently ascertained and adequately parameterised, and also provided that the vertical distribution of the algal biomass can be inferred from the partial information (restricted to the upper layer) delivered by ocean colour sensors.

CONTENTS

1. INTRODUCTION

During a given day the photosynthetically stored radiant energy within the productive column, $\overline{PSR}$ (MOREL, 1978) is, *a priori*, proportional to the daily photosynthetic available radiation at the surface PAR(0⁺) and to the algal biomass, as depicted by $<Chl>_{TOT}$, the column-integrated chlorophyll content, thus:

$$\overline{PSR} = \overline{PAR}(0^+) <Chl>_{TOT} \psi^* \quad (1)$$

with $\overline{PSR}$ and $\overline{PAR}(0^+)$ expressed in the same units, J $m^{-2}d^{-1}$; where the overbars mean daily integrated quantities and the notation 0^+ means "just above the surface" (see also Appendix 1); and $<Chl>_{TOT}$ as g m^{-2}. According to its dimension, the factor ψ* must be regarded as a cross section for photosynthesis per unit of chlorophyll pigment and expressed as m^2 (g Chl)$^{-1}$.

Such a purely phenomenological equation, would be of limited interest if ψ* was found to be widely and erratically variable. In MOREL (1978), ψ* was proven to vary within the range ±50%, around a central value equal to 0.07 m^2(g Chl *a*)$^{-1}$, in spite of highly contrasting trophic situations considered (oligotrophic Sargasso Sea waters, moderately productive waters in the eastern Equatorial Pacific and eutrophic waters in the Mauritanian upwelling area). This means that 7% of the visible (photosynthetic) radiation, or about 3% of the total solar energy, can be stored by photosynthesis when 1g of chlorophyll per square metre is present in the upper sunlit layer of the ocean.

By reversing the relationship between energy storage and carbon fixation (39 KJ per gC fixed)

and by expressing PAR(0^+) in terms of Einstein m^{-2}, i.e. mol of quanta m^{-2} (for this conversion the factor is 2.5 10^{18} quanta J^{-1}, a mean value for the underwater environment — see MOREL and SMITH, 1974) the above relationship can be rewritten as:

$$P = \overline{PAR}\ (0^+)\langle Chl\rangle_{TOT}\ \psi \qquad (2)$$

where P, in gC $m^{-2}d^{-1}$, is the net production, namely the amount of carbon added to the initial pool during the day in question, and where ψ, called the "light utilization index" by FALKOWSKI (1981), is expressed as g C(g Chl)$^{-1}$ (Einst m^{-2})$^{-1}$. The numerical conversion is effected through $\psi = 6.174\ \psi^*$, where the factor is not dimensionless. Therefore in correspondence to $\psi^* = 0.07$ (± 0.035) m^2(g Chl)$^{-1}$, ψ amounts to 0.44 (± 0.22) g C (g Chl)$^{-1}$ (Einst m^{-2})$^{-1}$. The validity of such a global and biogeochemical approach to marine photosynthesis, as well as the relative constancy of the parameter ψ were recently confirmed by PLATT (1986) who reviewed various studies, converting all the data into compatible and coherent units. The index ψ varies remarkably little in the studies considered by PLATT (comprising that of MALONE, 1987), its values ranging from 0.31 to 0.66 g C (g Chl)$^{-1}$ (Einst m^{-2})$^{-1}$, around the value (0.43) found by FALKOWSKI (1981) for the New York Bight. These ψ values are equivalent to ψ^* ranging from 0.05 to 0.106 m^2(g Chl)$^{-1}$. Higher values, however, have been recently published (YODER, ATKINSON, BISHOP, BLANTON, LEE and PIETRAFESA, 1985; CAMPBELL and O'REILLY, 1988). One quarter (54 out of 207) of the data points shown in Fig. 18 (MOREL, 1988) correspond to ψ^* values greater than 0.105 m^2 (g Chl)$^{-1}$; so a broader range for ψ^* will probably need to be acknowledged.

Nevertheless, this relative "stability" for a biological parameter related to a phenomenon subjected to a variety of environmental influences is at first sight surprising and deserves analysis. What we know about phytoplankton physiological responses at the algal cell level has to be combined with the possible changes in the surrounding conditions; among them are the spectral quality of the radiant energy available at the different levels within the productive column, the duration of the light period and also the physical conditions (stratification) which govern the nutrient availability and thus the vertical structure of the algal biomass and the chlorophyll to carbon ratio.

If both the mean value of ψ^* can be explained and its variations within a relatively restricted range can be accounted for, then a powerful "biogeochemical constant" becomes available for studying the carbon cycle and other related cycles, particularly at the global scale made accessible by satellite techniques.

2. ANALYSIS

2.1. *The net growth rate equation*

At a depth Z within the illuminated column, the local and instantaneous net production, dC(Z,t)/dt can be expressed as a function of the available radiant energy PAR(Z,t) according to (BANNISTER, 1974; KIEFER and MITCHELL, 1983):

$$dC(Z,t)/dt = \mu_c C(Z) = 12\ PAR(Z,t)\ \bar{a}^*\ Chl(Z)\ \varphi_\mu \qquad (3)$$

where C(Z) and Chl(Z) are the local carbon and chlorophyll concentrations (g m^{-3}), μ_c(time^{-1}) is

the net growth rate with respect to C, and $\bar{a}^*$, in m^2(g Chl)$^{-1}$, is the absorption cross section per unit of chlorophyll pertinent to the actual spectral composition. The product $\bar{a}^*$(Chl)PAR represents the energy absorbed by algae, (see Appendix 1). Finally φ_μ (MOREL, LAZZARA and GOSTAN, 1987) is a yield which expresses the efficiency in the transformation of the captured energy into carbon added to, and ultimately retained within, the initial carbon pool. The yield φ_μ differs from, and is lower than, the "physiological" quantum yield for photosynthesis, since a certain part of the carbon initially fixed is lost by respiration or excretion (the subscript μ indicates that the growth rate is exclusively involved). The factor 12 (g C/mol C) must be introduced if φ_μ is expressed as mol C per mol of (absorbed) quanta and in this case PAR must be expressed in terms of quanta per unit time. If the carbon fixation, dC(Z,t)/dt is converted into its energetic equivalent PSR(Z,t), equation (3) becomes:

$$PSR(Z,t) = 12\ PAR(Z,t)\ \bar{a}^*\ Chl\ (Z)\ \Phi_\mu \tag{4}$$

where Φ_μ which replaces φ_μ is now a dimensionless yield, and is simply defined as the ratio of stored energy to absorbed energy; the conversion is numerically achieved by using $\Phi_\mu = 1.943\varphi_\mu$, where the numerical factor is not dimensionless.

There are obvious structural similarities between equations 4 and 1 or equivalently between 3 and 2. Equation 1 is equation 4, once it has been time-integrated and depth-integrated. Moreover by comparing equations 1 and 4, the dimensionless character of Φ_μ is obvious and consistent with the fact that $\bar{a}^*$ as well as ψ^*, are both Chl-specific cross sections, respectively for absorption and for photosynthesis. Similarly integrating equation 3 with respect to time and depth would provide P in equation 2. Equations 3 and 4, however, are incomplete because spectral dependency of several quantities involved, is omitted; integration with respect to wavelength (λ) is also needed. Therefore, equation 3, has to be triply integrated according to

$$P = 12 \int_0^D \int_0^L \int_{\lambda 1}^{\lambda 2} Chl(Z)PAR(\lambda,Z,t)a^*(\lambda)\ \varphi_\mu(\lambda,Z,t)\ d\lambda\ dZ\ dt \tag{5}$$

to provide P, the daily realised column production; D stands for the depth of the productive layer, L for the length of the day and λ_1,λ_2, (generally 400 and 700 nm) for the limits of the photosynthetic spectral domain. P can straightforwardly be transformed into $\overline{PSR}$, as stated earlier (with 39 KJ/gC). If equation 5 is solved and $\overline{PSR}$ computed, the Chl-specific cross-section for photosynthesis, ψ^*, is easily derived as

$$\psi^* = \overline{PSR}/\overline{PAR}(0^+)\ \langle Chl\rangle_{TOT} \tag{6a}$$

with

$$\langle Chl\rangle_{TOT} = \int_0^D Chl(Z)\ dZ \tag{6b}$$

and

$$\overline{PAR}(0^+) = \int_0^L \int_{\lambda 1}^{\lambda 2} E_d(\lambda,0^+,t)\ d\lambda\ dt \tag{7}$$

where E_d is the downwelling PAR irradiance at the ocean surface (see appendix 1). The index ψ is derived from P by using the relevant units for $\overline{PAR}$ (0^+) (quanta instead of joules).

2.2. The depth-, time- and wavelength-dependent quantities

In equation 5 above the photosynthetic available radiation, PAR, obviously depends on the three variables, λ, Z and t; the pigment profile Chl(Z) could also be made time-dependent (to account for algal cell displacement) and $a^*(\lambda)$ made depth-dependent (to account for various algal populations in a stratified system). These kinds of dependencies are easily introduced if information exists, as for instance when simulating an actual and well documented situation. Such simulations are beyond the scope of the present study.

In principle, the quantum yield for growth depends upon the wavelength in so far as the action spectrum does not necessarily coincide with the absorption spectrum, but above all it depends on the radiation level, which itself changes with depth and time. It is believed, however, that φ_μ reacts to the amount of radiation which can be "seen" by the cells, or in other words, depends on the photosynthetically usable radiation PUR rather than on the available radiation PAR; PUR is a spectrally integrated quantity, defined as the fraction of radiant energy of such wavelengths that can be absorbed by algae (MOREL, 1978). At least in culture experiments, it has been demonstrated that φ_μ is more regularly ruled by PUR than by PAR when the spectral composition of light changes (MOREL *et al.*, 1987). There is no particular difficulty in using PUR when modelling the behaviour of φ_μ, since the computation of PUR makes a simultaneous use of the two variables already defined, PAR (λ) and a*(λ), according to:

$$PUR\ (\lambda) = PAR\ (\lambda)\ a^*(\lambda)\ (a^*_{max})^{-1} \tag{8a}$$

where a^*_{max} is the maximal value of a*(λ), generally occurring at λ about 440 nm. The integrated PUR value, on which φ_μ depends, is therefore

$$PUR = (a^*_{max})^{-1} \int_{\lambda 1}^{\lambda 2} PAR\ (\lambda)\ a^*(\lambda)\ d\lambda \tag{8b}$$

and remains a depth and time-dependent energy, denoted PUR (Z, t).

2.3. Chlorophyll-specific cross sections for absorption and for photosynthesis

Another point needing clarification is that of the absorbed radiation by algae, thereafter denoted ARA. This amount of energy, which depends on the three variables, corresponds to the product

$$ARA\ (\lambda, Z, t) = a^*(\lambda)\ Chl\ (Z)\ PAR(\lambda, Z, t)$$

which is a part of equation 5. As discussed in Appendix 1, the adequate radiometric quantity, which depicts the in-water radiant energy available for photosynthesis (PAR) is the scalar irradiance, $\mathring{E}$. The amount of absorbed energy per unit of volume is strictly expressed as the product $a.\mathring{E}$ (the so-called Gershun equation), where a is the absorption coefficient (m^{-1}). When dealing only with algae and if only algal absorption is to be computed, the absorption coefficient, a (λ), is the product a* (λ) Chl (Z).

Irradiance, however, is generally measured, or will be modelled below, in terms of downwelling irradiance, E_d. Since E_d is always an underestimate of the scalar irradiance $\mathring{E}$, a "geometrical" corrective term is necessary, which will be expressed later (equations 17 to 21).

By assuming that this correction is feasible and PAR correctly evaluated, the following integration can be performed

$$ARA = \int_0^D \int_0^L \int_{\lambda 1}^{\lambda 2} ARA\,(Z,t,\lambda)\, dZ\, dt\, d\lambda \qquad (9)$$

and provides the total amount of energy absorbed by algal cells present in the water column and during the entire day. By strict analogy with equation 1, ARA can be written:

$$ARA = \overline{PAR}(0^+) <Chl>_{TOT} A^* \qquad (10)$$

where A^* in m^2 (g Chl)$^{-1}$ is a "mean" absorption cross section per unit of Chl *a*, valid for the whole productive column, the entire light period and the entire photosynthetic spectrum. By dividing equation 1 by equation 10 the dimensionless number Φ^* is produced:

$$\Phi^* = \psi^* / A^* \qquad (11)$$

which expresses the "mean" yield in the global conversion of absorbed energy into stored energy within the productive column for the day in question. It is a time and depth-averaged value of the dimensionless yield Φ_μ which was previously defined above on a local and instantaneous basis (equation 4).

2.4. A simplified case

Before extensively using equation 5 as a tool in a modelling study, its links with the integrated quantities which appear in equations 1 or 2 can be made simpler by using the assumptions summarized below:

(i) $Chl(Z) = Chl$

(ii) $a^*(\lambda) = \bar{a}^*$

(iii) $PAR(Z, t) = \overline{PAR}(0^+, t)\, e^{-\bar{K}Z}$

These assumptions allow the various terms in equation 5 to be separately integrated. They presume the following: (i) pigment is uniformly distributed;(ii) a spectrally-averaged and constant Chl-specific absorption coefficient, $\bar{a}^*$, can be adopted, (iii) the available polychromatic irradiance decreases exponentially for increasing depth with a unique attenuation coefficient denoted $\bar{K}$. With the above approximations the integration of equation 5 (see Appendix 2) provides:

$$P = (12/4.6) <Chl>_{TOT} \overline{PAR}(0^+)\, \bar{a}^* \bar{\varphi}_\mu \qquad (12)$$

where

$$\bar{\varphi}_\mu = \int_0^{Ze} \int_0^L \int_{\lambda 1}^{\lambda 2} \varphi_\mu\,(\lambda,Z,t) d\lambda\, dZ\, dt$$

represents a "mean" quantum yield valid for the euphotic layer (depth Z_e), for the entire light period and the entire visible spectrum. A comparison between equations 12 and 2 clearly shows that:

$$\psi = (12/4.6)\, \bar{a}^*\, \bar{\varphi}_\mu \qquad (13a)$$

a relationship which has already been established by PLATT (1986, his equation 16) through an apparently, albeit not basically, different approach. Using the conversion factors previously given, this relationship can also be transformed into:

$$\psi^* = (1/4.6)\, \bar{a}^*\, \Phi^* \qquad (13b)$$

Using the value derived above for ψ^*, $0.07 m^2(g\ Chl)^{-1}$, and BANNISTER's value (1974) for $\bar{a}^* = 16 m^2(g\ Chl)^{-1}$, it follows that $\Phi^* = 0.02$ or $\bar{\varphi_\mu} = 0.01$ mol C per Einstein absorbed. This value is quite reasonable and compatible with our present knowledge about the *in situ* net quantum yield and its variations with depth (see e.g. BANNISTER and WEIDEMANN, 1984). The only merit of this drastically simplified approach is to reconcile the physiological parameters with the bulk geochemical index ψ^*. The following study aims at carrying out similar computations in the general case, without using oversimplifying assumptions as above.

Computations of this kind rely on a systematic use of equation 5 with an appropriate parameterisation of all the quantities involved. In other words, around a core formed by this equation, is built a light-photosynthesis model which accounts for the climatological aspect of the radiant energy availability at the top of the productive layer, for the penetration of the photosynthetically active radiations within this layer (a penetration which depends, in oceanic Case 1 waters, on the algal biomass itself), and lastly for the absorption by algae of these radiations resulting in a net carbon fixation. Toward this objective bio-optical models for computation of *in situ* phytoplankton production have been developed by BIDIGARE, SMITH, BAKER and MARRA (1987) and very recently by SATHYENDRANATH, PLATT, CAVERHILL, WARNOCK and LEWIS (1989).

Such a time, depth, wavelength-dependent model can be seen as a sub-model to be used for the more general purpose of describing or predicting the algal biomass evolution. When embracing this problem in its entirety (see, e.g. JAMART, WINTER, BANSE, ANDERSON and LAM, 1977) nutrient consumption and regeneration, vertical mixing, sinking and grazing are other phenomena which will need to be modelled, in addition to the processes of light capture and utilisation, restrictively considered here. However, in ecological models the initial photosynthetic process is in general poorly modelled because of oversimplifying parameterisations. It is believed that substantial improvements are presently within our reach.

3. PROCESSES TO BE MODELLED

3.1. *Modelling PAR (λ,t) just above and just below the surface*

The extra-terrestrial solar radiation at the mean sun-earth distance is taken from NECKEL and LABS (1984). For each Julian day considered, the solar flux is corrected for the ellipticity of the terrestrial orbit according to the formula given by SPENCER (1971). For each particular day the declination of the sun is computed (SPENCER, 1971) and then combined with the latitude of the selected location to obtain the solar elevation as a function of time and also the daylength.

A radiative transfer model, directly derived from that developed by TANRÉ, HERMAN, DESCHAMPS and DE LEFFE (1979) is used to compute the direct solar radiation and the diffuse sky radiation impinging on a horizontal surface at the sea level. Standard profiles of temperature and ozone (MCCLATCHEY, FENN, SELBY, VOLZ and GARING, 1971) are used. For the spectral range considered, variable amounts of water vapor have no significant influence on the integrated

(400-700nm) PAR value. Thus PAR is reduced by -0.7% or -3% when the precipitable water content increases from 0.5 to 5cm, respectively when the sun is at Zenith, (θ=0°), or near the horizon (θ=80°). The standard run is effected with 2cm of precipitable water. Through its weak absorption in the green part of the spectrum (Chappuis band), ozone perceptibly influences integrated PAR. For a total ozone content varying from 250 to 450 DU, PAR is decreased by about 1% or 10% respectively for θ=0° or 80°. A value of 350 DU is adopted for the standard run. More crucial is the effect of the tropospheric aerosol load. With aerosols of the "marine type" (WORLD CLIMATE PROJECT, 1983) and visibilities, V, diminishing from 50 to 5km, the PAR value is reduced by 5.9% for θ=0° or by 22% if θ=80°. Another important feature is the relative increase of the diffuse radiation which, for instance, can overtake the direct radiation, whatever the sun altitude and wavelength, when the visibility is 5km (see Fig. 1a). For standard runs simulating clear skies V is taken to be 23 km (see Fig. 1b).

The transmission across the air-water interface is separately computed for the diffuse irradiance component $E_{sky}(\lambda)$, by using a constant reflectance (6.6%), and for the direct component, $E_{sun}(\lambda)$, by using a sun-altitude dependent reflectance. The wave slopes, which depend on the wind speed, modify the Fresnel coefficients which are strictly valid for specular reflection on perfectly smooth ocean surfaces. The reflectance values tabulated by AUSTIN (1974) for wind speeds ranging from 0 to 16 m s^{-1} are used for simulations and a value of 4m s^{-1} is selected for the standard run. By integrating E_{TOT} with respect to wavelength and time where $E_{TOT}(\lambda,t) = E_{SKY}(\lambda,t) + E_{SUN}(\lambda,t)$, the daily photosynthetic available radiation just above the surface denoted PAR (0^+) can be obtained. In Fig.2, PAR (0^+) is shown as a function of latitude (north) and for the days of the summer solstice. Similar integrations, once the correction for reflection is applied, lead to PAR (0^-), just below the surface. For the entire day in question, the loss by reflection amounts to 4.5% from the equator to the mid-latitudes and reaches 7.6% at 80°N. Values close to 9% are obtained when the sun has a lower elevation, as in winter at high latitudes. The wind speed has only a minute influence, hardly discernible with the scale used in Fig.2. It must be acknowledged, however, that computation is somewhat inaccurate when the sun is very low since wave orientation is not considered with respect to the sun's azimuth. Results in PREISENDORFER and MOBLEY (1986) should enable a more precise treatment of this process, if needed.

For further use μ_o, the value of the average cosine for downwelling radiation, just below the surface, is computed as

$$\mu_o(\lambda) = [\mu_{sun} E_{sun}(\lambda) + \mu_{sky} E_{sky}(\lambda)] / E_{TOT}(\lambda) \qquad (14)$$

where μ_{sun} is the cosine of the sun-zenith angle after refraction and μ_{sky}, also sun altitude dependent, by approximation is considered as being a constant equal to 0.86. Figure 3 shows, for some selected wavelengths, how μ_0 varies with the sun zenith angle (measured in air, before refraction).

Above the sea surface the spectral composition of the direct and diffuse radiations, as well as their respective importance, vary significantly with the elevation of the sun. Just below the surface, these features are modified by the distinct reflectances which affect the two components separately. A simple result, however, appears (Fig.1c) which allows a simplified version of the above calculation to be used without losing the final accuracy. Once transmitted through the interface, the spectral values of total irradiance (sun + sky) are practically linear functions of $(\cos\theta)^{1.2}$, independent of the atmospheric turbidity. This result is very close to the experimental determinations made by HØJERSLEV (1980) leading to a $(\cos\theta)^{1.4}$ dependency, but in contradiction with the expression $(\cos\theta)^3$ proposed by IKUSHIMA (1967). The $(\cos\theta)^{1.2}$ function, combined with

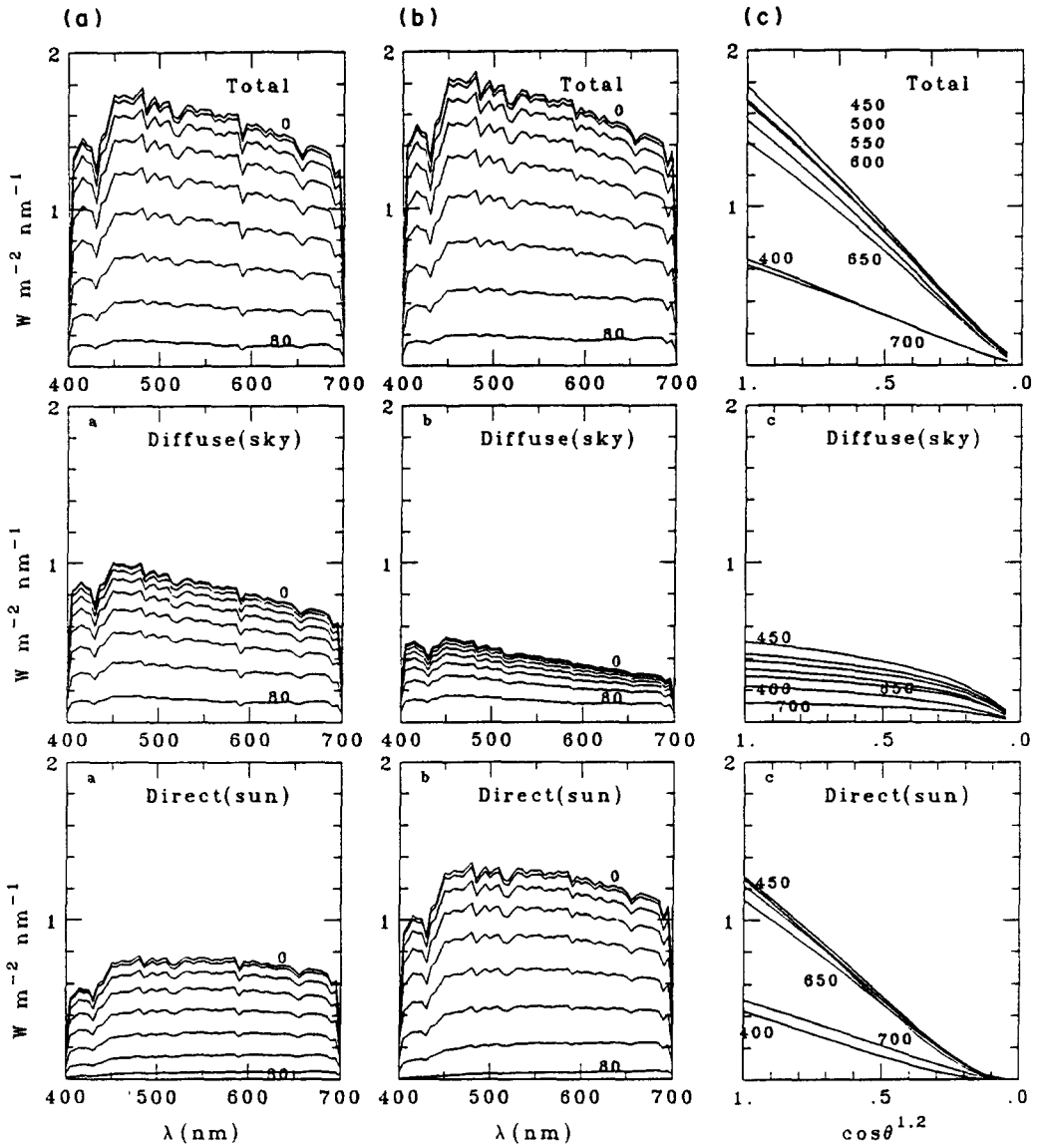

FIG. 1. Spectral distribution of the downwelling irradiance just above the ocean surface for various sun-zenith distances ranging from 0° to 80° (by 10° increments). Total irradiance, diffuse and direct components are shown. The left panels (a) are for a visibility V = 5km, a precipitable water content of 2cm and an ozone content of 350 DU; the panels in the middle (b) are for V = 23 Km, (H_2O) = 0.5 cm and (O_3) = 350 DU (=0.35 cm atm). In the Fig. 1(c), the conditions are those of Fig.1(b). For some selected wavelengths as indicated (nm), the downwelling irradiance values computed just below the surface (wind speed 4 ms^{-1}) are plotted as a function of $(\cos\theta)^{1.2}$.

a typical spectrum $E_{TOT}(\lambda)$ at noon, can form the basis of a simplified model (actually used in preliminary sensitivity tests).

3.2. *Propagating the downwelling irradiance through the water column*

Given the spectral distribution of the irradiance just below the surface E_d (λ,0$^-$, t) and the chlorophyll vertical profile Chl (Z), the depth of the euphotic zone, at t_0 = noon, is determined by

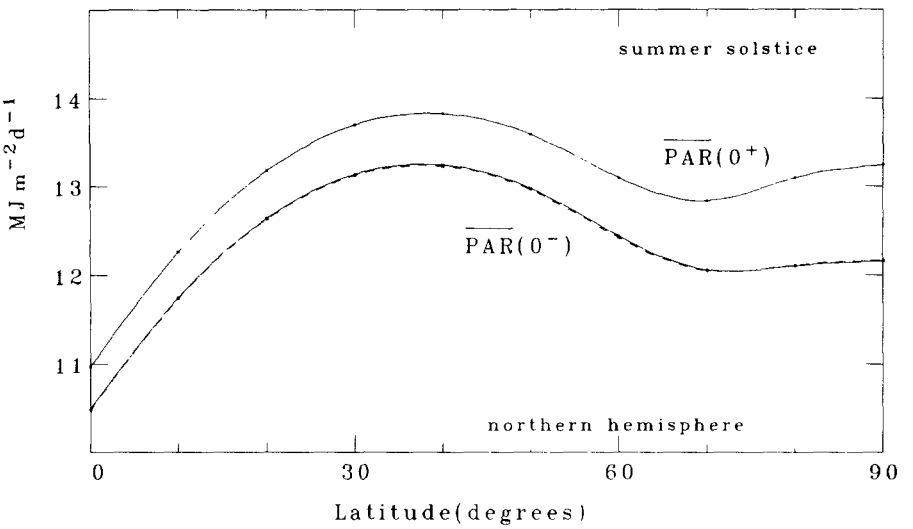

FIG. 2. Daily total (direct + diffuse) downwelling irradiance just above and just below the surface, PAR (0^+) and PAR (0^-), as a function of latitude in the northern hemisphere and for the summer solstice. The two (barely distinguishable) PAR (0^-) curves correspond to wind speeds of 4 and 16 ms^{-1}(solid and dashed curves, respectively).

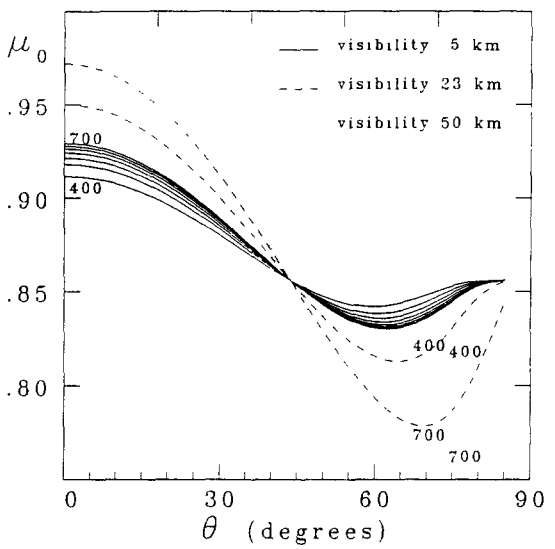

FIG. 3. Average cosine for downwelling radiation just below the surface - $\mu_0(\lambda)$ in equation 14 - and for λ = 400 (50) 700 nm, as a function of θ, the sun-zenith angle in air. Wind speed is 4 ms^{-1} and visibility, V, is 5, 23 and 50 km as indicated. For V = 23 and 50 km, only the curves for 400 and 700 nm are shown.

a preliminary computation. With a judiciously chosen depth interval dZ, ranging from 0.05 to 0.5m according to the chlorophyll concentration profile, the downwelling irradiance, is computed from the surface as:

$$E_d(\lambda, Z_n+dZ, t_0) = E_d(\lambda, Z_n, t_0)\, e^{-K_n(\lambda)\,dZ} \qquad (15)$$

where the first Z_n value is zero. The spectral attenuation coefficient for downwelling irradiance, $K_n(\lambda)$, which depends on the chlorophyll concentration $(Chl)_n$ within the layer extending from Z_n to $Z_n + dZ$, is obtained from:

$$K_n(\lambda) = K_w(\lambda) + \chi(\lambda)\,(Chl)_n^{e(\lambda)} \tag{16}$$

The validity of this equation is restricted to Case I waters, where nothing besides algae, with their associated retinue, can influence the optical properties. $K_w(\lambda)$ stands for the influence of pure water; the factors $\chi(\lambda)$ and the exponents $e(\lambda)$ were obtained through regression analyses (MOREL, 1988: the tabulated values of $K_w(\lambda)$, $\chi(\lambda)$ and $e(\lambda)$ are given in this reference). At each level, and by integrating with respect to λ (between 400 and 700nm), the amount of photons is computed and compared to that existing just above the surface (0^+). The depth of the euphotic layer, Z_e, is determined (within $\pm$ dZ) when the residual downwelling photon flux is reduced to 1/100 of the initial value. This computation conforms to the most common definition of Z_e (see Appendix 1).

For further computations, a potentially "productive" column is defined as being 1.5 times thicker than the above computed euphotic zone and this column is subdivided into 100 discrete layers of equal thickness dZ (different from the previous one). At the 100 levels, the $E_d(\lambda,Z,t)$ values and the spectral integrated values are computed. They are varied during the day by using, as input values, the products of the preceding atmospheric model. For that, the time increment is set equal to 1/60th of the day length (i.e. 12 minutes for L=12h).

3.3. *Absorbed radiation by the algae*

Given that a chlorophyll-specific absorption spectrum for algae $a^*(\lambda)$ can be selected (see below "choice of physiological parameters"), the partial absorption coefficient resulting from the presence of algae, with a local chlorophyll concentration (Chl), is $a_{Chl} = a^*(Chl)$ (the arguments λ and Z are omitted for what follows). The absorbed energy (see Appendix 1) is given by the product $a_{Chl}\,\mathring{E}$, where $\mathring{E}$ is the scalar irradiance, different from, and always superior to, the downwelling irradiance (E_d) computed in the preceding section. The exact relationship which links these irradiances is (see e.g. PREISENDORFER, 1976):

$$a\,\mathring{E} = K_d\,E_d\,[1 - R\,(K_u/K_d)] \tag{17a}$$

$$a\,\mathring{E} \sim K_d\,E_d \tag{17b}$$

where K_d and K_u are the attenuation coefficients for the downwelling and the upwelling irradiances respectively and R is the reflectance, defined as E_u/E_d, the ratio of upwelling to downwelling irradiance. In general, K_u does not widely differ from K_d, moreover R is only of the order of a few percent. Therefore the absorbed energy can be safely expressed through the product $K_d\,E_d$ instead of $a\,\mathring{E}$ (equation 17b). A problem still remains in so far as that part of K_d which is caused only by the algal cells is unknown. Note that when regressing K_d against (Chl), a "chlorophyll-specific" attenuation coefficient can be produced (the so-called "k_c" coefficient) and the contribution of algae in forming K_d should be the product $k_c(Chl)$. In the natural environment, however, the living algae are inevitably associated with detritus, thus the k_c value, as derived from field data and regression analysis, necessarily combines the effects of algal cells

and all co-varying substances (see discussion about k_c in MOREL, 1988). The same drawback occurs when relating the absorption coefficient of natural waters to their chlorophyllous pigment content (PRIEUR and SATHYENDRANATH, 1981).

It is postulated at this stage that a "true" absorption spectrum for only living algal cells can be adopted and will be used in later computations (see "input parameters"). Since this absorption coefficient must be multiplied by $\mathring{E}$ (and not combined with E_d), it is therefore necessary to know the ratio $\mathring{E}/E_d$, or equivalently the ratio K_d/a. Estimating this ratio, in principle, requires a complete solution of the radiative transfer problem. The considerable uncertainties attached to the physiological parameters leaves one to think however, that approximate solutions of the radiative transfer are sufficient.

In essence, K_d/a is a non-explicit function of the radiance distribution above the surface, of the depth and of the inherent optical properties of the medium, namely its absorption and scattering coefficients, a and b, and its volume scattering function. Through Monte Carlo calculations, KIRK (1984) was able to show that the average value of K_d throughout the euphotic zone can be expressed as:

$$K_d = a\,\mu_0^{-1}[1 + (0.425\mu_0 - 0.19)\,b/a]^{1/2} \tag{18}$$

where μ_0 is the average cosine for downwelling radiation just below the surface (see equation 14). Rather than depth-dependent relationships, this global approximation can be used for the entire productive column. To use this expression, $b(\lambda)$ and $a(\lambda)$ are modelled as a function of the chlorophyllous pigment content according to:

$$b(\lambda) = b_w(\lambda) + (550/\lambda)\,0.3\,(Chl)^{0.62} \tag{19}$$

$$a(\lambda) = [a_w(\lambda) + 0.06\,A_{Chl}(\lambda)\,(Chl)^{0.65}]\,[1+0.2y(\lambda)] \tag{20a}$$

with

$$y(\lambda) = \exp[-0.014\,(\lambda - 440)] \tag{20b}$$

Equation 19, given in GORDON and MOREL (1983), allows particle scattering to be inversely related to the wavelength and non-linearly related to the pigment content. Equation 20a and the $A_{Chl}(\lambda)$ tabulated values come from PRIEUR and SATHYENDRANATH (1981). The spectral values of the scattering and absorption coefficients for optically pure sea water, $b_w(\lambda)$ and $a_w(\lambda)$, are found in MOREL (1974) and MOREL and PRIEUR (1977) respectively. Note that the exponent (0.65) appearing in equation 20a is slightly modified with respect to that given by PRIEUR and SATHYENDRANATH (0.60). By this way the $K_d(\lambda)$ values produced by equation 18 are fully consistent (Fig.4a) with those derived from direct statistical analysis (equation 16). The second bracket in equation 20a accounts for a co-varying influence of "autochthonous" yellow substance, expressed through equation 20b (BRICAUD, MOREL and PRIEUR, 1981).

It is worth noting that the derivation of equation 20a with respect to (Chl) should produce a "chlorophyll-specific" absorption coefficient, to the extent that it would be constant. It is, however, varying as $(Chl)^{-0.35}$. As said before, the reason for this non-constancy is the influence of other materials (detrital or microbial) covarying with, albeit not linearly related to, the living algae. Therefore such a variable coefficient is inadequate when computing the amount of radiation actually absorbed by only living algae. Conversely, the global effect of algal biomass (including its breakdown products) upon the absorptance within the medium is adequately

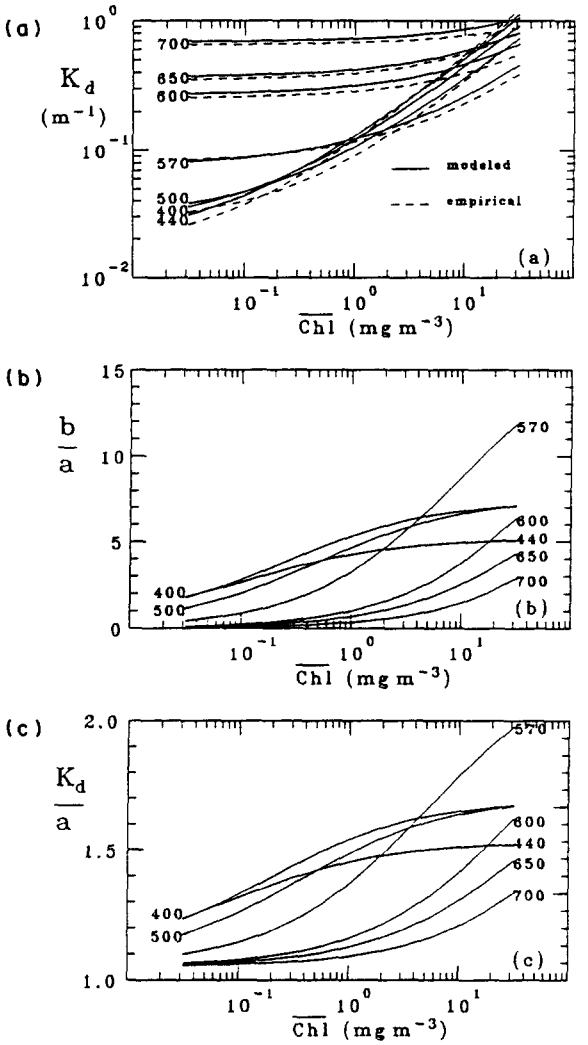

FIG. 4(a). Variations of K_d (λ) for selected wavelengths (nm), as a function of the chlorophyll concentration. Solid curves are for K_d (λ) values computed through equation 18 to 20b, and dashed curves for K_d (λ) derived from statistical study of field data (equation 16).
FIG. 4(b). Variations of the ratio b/a (scattering-to-absorption, equation 19 and 20) for the same λ as in 4a, as function of the chlorophyll concentration.
FIG. 4(c). Variations of the ratio $K_d/a(=\mathring{E}:E_d)$.

reproduced by an expression like equation 20a.

Since the present study is restricted to Case I waters, no other allochtonous (terrigeneous) components are considered when computing a(λ) or b(λ). The b/a values for some selected wavelengths are plotted vs. (Chl) in Fig. 4b and the corresponding $\mathring{E}/E_d$(=K_d/a) values, in Fig. 4c.

This ratio $\mathring{E}/E_{d'o}$ hereafter noted as g(λ,t,Chl), will be used as a "geometrical" correction to transform E_d into $\mathring{E}$. The λ-dependency implicitly involves the pigment concentration (through equations 19 and 20).

As the K_d(λ) values produced by equation 18 are mean values for the whole euphotic layer, it is consistent within the same approximation to consider and use the average pigment

concentration for this layer computed as $\overline{Chl} = Z_e^{-1} \int_0^{Ze} Chl(Z)\, dz$. The dependency of g upon time replaces that upon μ_0 via equation 14, where μ_0 is produced from time-varying quantities.

The E_d (λ,Z,t) values previously computed are converted into $\mathring{E}$ (λ,Z,t) = PAR (λ,Z,t) according to:

$$PAR(\lambda,Z,t) = E_d(\lambda,Z,t)\, g(\lambda,t,Chl) \tag{21a}$$

and the PUR (λ, Z, t) values (see also equation 8b) according to

$$PUR(\lambda,Z,t) = E_d(\lambda,Z,t)\, g(\lambda,t,Chl)\, a^*(\lambda)\, (a^*_{max})^{-1} \tag{21b}$$

3.4. *Modelling the quantum yield for growth $\varphi_\mu(\lambda,Z,t)$*

There is recent evidence to show that the photosynthetic action spectrum nearly reproduces the absorption spectrum (LEWIS, WARNOCK, IRWIN and PLATT, 1985). In the absence of contradictory and more precise information, the wavelength dependency of φ_μ will be ignored. As said in the introduction, it seems reasonable to consider φ_μ as a dependent variable of the total usable radiation, PUR(Z,t), computed by integrating equation 21b over the 400-700nm domain.

This yield experiences its maximum, $\varphi_{\mu max}$, at vanishing irradiances and decreases when the light level increases (note that $\varphi_{\mu max}$ is a maximal yield for net growth and not the maximum yield for photosynthesis, as used by physiologists). From a computational point of view it is advantageous to express φ_μ as a function of a dimensionless parameter, x, defined as being

$$x = PUR/KPUR$$

the ratio of actual PUR to a certain normalising value, denoted KPUR; the normalisation is discussed below. By introducing a function f(x) which, from a value of 1 when x = 0, monotonously decreases when x increases, and tends toward 0 when x tends to infinity, φ_μ can be written as,

$$\varphi_\mu(x) = \varphi_{\mu max}\, f(x) \tag{22a}$$

This concise formulation is to be related to the parameters commonly defined from the "light-photosynthesis" curve, also called the "P^B vs I" curve, where I is in general PAR, or alternatively can be PUR, and P^B is the net photosynthesis (the amount of carbon fixed) per unit of chlorophyll biomass and per unit of time, thus

$$P^B = \frac{dC}{dt}(Chl)^{-1}$$

By using equations 3 and 8b

$$P^B = 12\, a^*_{max}\, PUR\, \varphi_\mu$$

which, combined with equation 22a, gives

$$P^B = 12\, a^*_{max}\, \varphi_{\mu\, max}\, KPUR\, [x.\, f(x)] \qquad (22b)$$

The evolution of P^B with changing PUR-irradiances is ruled by the dimensionless bracketed product [x.f (x)], whereas its magnitude is governed by the physiological parameters a^*_{max}, $\varphi_{\mu max}$ and KPUR. An important parameter of the P^B vs I curve is the maximal value P^B_{max}, which is simply determined by $[x.f(x)]_{max}$, the maximal value attainable by this product.

The other important parameter of the P^B vs. I curve is its initial slope. When I is PUR, the initial slope becomes independent from the spectral composition of the ambient light and takes a maximal (and unique) value, denoted α' (as in Morel *et al* ., 1987) ; α' is expressed as:

$$\alpha' = P^B/PUR \text{ when } PUR \rightarrow 0$$

By using equation 22b and noting that f(x) is identically equal to 1 when x tends toward 0, it becomes:

$$\alpha' = 12a^*_{max}\, \varphi_{\mu\, max} \qquad (22c)$$

The structure of the function f(x) can be straightforwardly derived from various expressions proposed in the literature to describe the P^B vs I curve. It is therefore necessary to define the normalizing irradiance KPUR. With monotonous functions, there is a single x-value, $x_{1/2}$, for which $f(x_{1/2})=1/2$, so that at this point φ_μ is half of its maximum. Physically this halving occurs at a given energy level, i.e. at a given PUR value, denoted $PUR_{1/2}$ (it is worth noting that $PUR_{1/2}$ is one of the physiological parameters to be selected). Now KPUR is defined as

$$KPUR = PUR_{1/2}/x_{1/2}$$

and provides the appropriate scaling for the various f(x) functions envisaged below. Among several available P^B vs I formulations, the following are selected.

3.4.1. *Michaelis-Menten-Monod type.* This type, adopted by Kiefer and Mitchell (1983), is re-written as:

$$f(x) = (1 + x)^{-1} \qquad (23)$$

For this expression $x_{1/2} = 1$ and P^B tends toward maximal value, P^B_{max}, when x tends to infinity and is proportional to the product $[x.f(x)]_{max}$, itself equal to 1.

3.4.2. *Steele type (1962).*

$$f(x) = e^{-x/e} \qquad (24)$$

for which $x_{1/2} = 1.884$; P^B experiences a maximum for x = e, with $[x.f(x)]_{max} = 1$, and thereafter decreases (inhibition simulation). This light-dependence function was adopted in the model developed by Jamart *et al* . (1977).

3.4.3. *Webb type (1974).*

$$f(x) = x^{-1}(1-e^{-x}) \tag{25}$$

leading to $x_{1/2} = 1.595$ and $P^B = P^B_{max}$ when $x \rightarrow \infty$, with P^B_{max} proportional to $[x.f(x)]_{max} = 1$.

3.4.4. *Platt type (1980).*

PLATT, GALLEGOS and HARRISON (1980) proposed a modification of Webb's expression with a view to reproducing the inhibition at high irradiance. From their expression it follows that:

$$f(x) = x^{-1}\,(1 - e^{-x})\,e^{-\beta x} \tag{26}$$

$\varphi_\mu = 1/2\ \varphi_{\mu\,max}$ is found for an $x_{1/2}$ value which is the solution of a transcendental equation and depends on ß (e.g. $x_{1/2} = 1.495$ if ß = 0.025). P^B is maximum for $x = \ln[(1+ß)/ß]$ (e.g. for $x = 3.714$ if ß = 0.025), and is proportional to $[x.f(x)]_{max} = ß^ß(1+ß)^{-(1+ß)}$ (e.g. to 0.889 if ß = 0.025; see details in Table 1).

The advantage of the Platt expression lies in the fact that the importance of photoinhibition can be adjusted through the parameter ß, whereas with Steele's type the (rather strong) inhibition is immutable. The normalized yield, i.e. $f(x) = \varphi_\mu/\varphi_{\mu\,max}$, and the dimensionless production, i.e. [x.f(x)], are shown as functions of the normalized irradiance x, on Figures 5a and 5b.

At least from a computational viewpoint there is no particular difficulty in simulating stratified situations with algal populations adapted to their depth (and light) levels. Such adaptation consists of modifying the P^B vs I curve, with generally diminishing P^B_{max} values at low light levels. This effect can be simply accounted for (eq.22b) by allowing KPUR to diminish for increasing depth. The possible change in the initial slope of the P^B vs I curve is easily simulated (eq.22c) by changing the a^*_{max} values, to the extent that $\varphi_{\mu\,max}$ could be assumed to be independent from species and adaptative states. The effect of temperature on photosynthesis, essentially characterized by the depressed values of P^B_{max} at lower temperature, can be similarly reproduced by the adoption of a relationship linking KPUR to the temperature.

TABLE 1. Relevant parameters used in the yield-irradiance relationship

Types	$x_{1/2}$	KPUR $\mu E\ m^{-2}s^{-1}$	$(x.f(x))_{max}$	P^B_{max} $gC\ (gChl)^{-1}h^{-1}$
MMM	1	40	1	3.42
S	1.884	21.23	1	1.82
P				
β =0.025	1.495	26.76	0.889	2.04
β=0.010	1.552	25.77	0.945	2.08
β=0.005	1.573	25.44	0.969	2.11
W	1.595	25.08	1	2.14

The abbreviations MMM, S, P, W stand for Michaelis-Menten-Monod, Steele, Platt *et al.* and Webb types (equations 23 to 25). The normalizing value KPUR varies in such a way that PUR = 40 $\mu Em^{-2}s^{-1}$, whatever the function adopted (equations 23 to 26). P^B_{max} is computed according to equation 22b where $\varphi_{\mu max}$=0.06 (molC/Einst absorbed) and a^*_{max}=33m² $(gChl\ a)^{-1}$. The temperature is assumed to be 20°C.

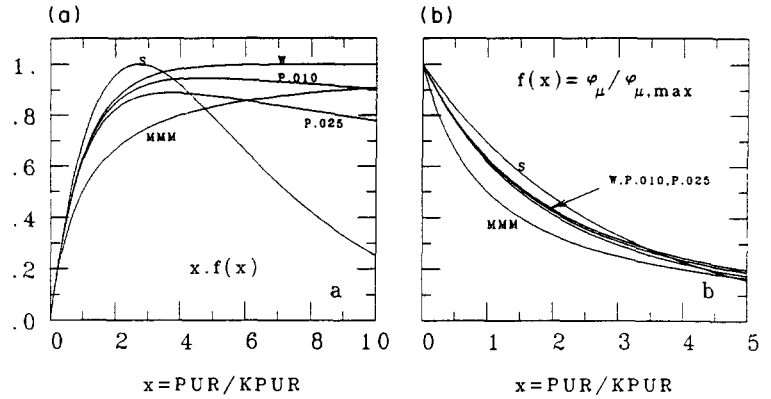

FIG. 5(a). Various production vs. irradiance curves represented in a dimensionless way (P/P_{max}, see text); irradiance is normalized with respect to a given irradiance level, KPUR (x = PUR/KPUR).
FIG. 5(b). The evolutions, as a function of x, of the quantum yield for growth, when normalized with respect to its maximal values at null irradiance. The abbreviations MMM, S, W, P.010, P.025 stand for Michaelis-Menten- Monod, Steele, Webb and Platt types with β= 0.010 and 0.025 (equations 23 to 26).

4. THE MODEL

4.1. *The global equations*

By reassembling the components examined separately above, equation 5, which provides the daily column production, can now be written:

$$P = 12\, a^*_{max}\varphi_{\mu\,max} \int_0^D \int_0^L \int_{\lambda 1}^{\lambda 2} Chl(Z)\, PUR(\lambda,Z,t)\, f[x(Z,t)]\, d\lambda\, dZ\, dt \qquad (27)$$

where the dimensionless irradiance x is a function of depth and time according to

$$x(Z,t) = KPUR^{-1} \int_{\lambda 1}^{\lambda 2} PUR(\lambda,Z,t)\, d\lambda \qquad (28)$$

and where f(x) is, as an option, one of the four expressions given above (equations 23 to 26). Recall that PUR(λ,Z,t) is an implicit function of Chl(Z) through equations 15 and 16 which have produced E_d, and also through equation 21b which has accounted for the geometrical effect, expressed through the term g (λ,t,Chl).

The cross section for photosynthesis per unit of integrated pigment ψ^* (equation 1) and the light utilisation index ψ (equation 2) can be obtained by combining P, with $\langle Chl \rangle_{TOT}$ and $\overline{PAR}$ (0^+) (equations 6 and 7).

The daily incident energy, $\overline{PAR}(0^+)$, is expressed either in KJ $m^{-2}d^{-1}$ or in Einstein $m^{-2}d^{-1}$, according to how ψ^* or ψ is to be computed. The production P and the areal pigment value $\langle Chl \rangle_{TOT}$ can also be computed for an "extended" productive layer (D=1.5 Z_e), because the somewhat arbitrary definition of Z_e leads one to presume that carbon fixation does not necessarily cease below this level.

4.2. *The variables and the input parameters*

The parameters used as inputs in the model belong to three categories:

(i) The environmental parameters, namely location, date, atmospheric (aerosol) conditions, wind speed, and sea-temperature T (possibly a temperature profile).

(ii) The ecological parameter, i.e. the chlorophyll vertical profile.

(iii) The physiological parameters, namely the chlorophyll-specific absorption spectrum $a^*(\lambda)$, the maximum yield for growth $\varphi_{\mu\,max}$, the yield-irradiance function f(x), the irradiance $PUR_{1/2}$, that value of PUR which corresponds to a yield reduced to half of its maximum value; $PUR_{1/2}$ together with f(x) determine the light-dependency of the carbon fixation; and finally the KPUR-T relationship.

Given a set of ecological and physiological parameters, the evolution of the production, P and of the cross-section ψ^* in response to environmental changes are unambiguously derived, since the physics involved is rather accurately modelled. More flexible, or arbitrary, is the choice of the physiological parameters which are less well documented. According to equation 27, however, there is no need for sensitivity studies with respect to a^*_{max} and $\varphi_{\mu\,max}$, which linearly control P, when all other parameters are fixed. The influences of $PUR_{1/2}$ and f(x) are by nature non-linear and can only be assessed through the full use of the model. In the same way the production capability of an algal biomass, when variously distributed along the vertical, can only be predicted by operating the model.

4.3. *Choice of plausible physiological parameters*

As discussed before, the light harvesting capacity of algae, depicted by a chlorophyll-specific absorption spectrum $a^*(\lambda)$, cannot be easily derived from field measurements, because of the presence of associated absorbing detritus (but see BIDIGARE *et al.*, 1987). Therefore, it seems reasonable to adopt spectral absorption values, pertaining to the phytoplankton alone, such as have been determined for cells grown in culture experiments. An average spectrum computed

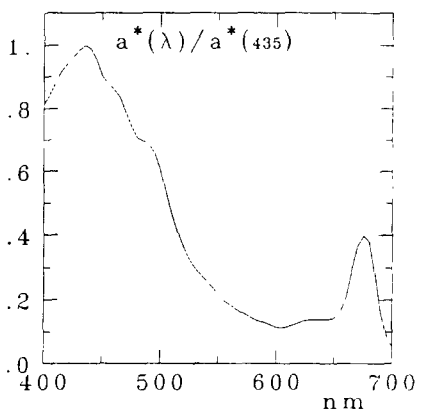

FIG. 6. Chlorophyll-specific absorption spectrum of intact living algal cells in relative units (normalized with respect to the maximum value at λ= 435nm. This mean spectrum has been computed by averaging actual spectra obtained for pure algal cultures (see references in MOREL, 1988).

from measurements for 14 species, grown in culture (the cyanobacteria being disregarded) is adopted (see Fig.6). The magnitude of individual spectra for the various species can vary within at least a factor 2, whereas the spectral shape, in a first approximation, is much less variable. If this shape is assumed to be unvarying and correctly represented by the average spectrum, no additional computations are needed when the absorption capabilities are changed since P is simply proportional to a^*_{max}. The a^*_{max} value used in a standard run is $33m^2$ $(gChla)^{-1}$ and occurs at $\lambda = 435nm$.

The maximal value of the quantum yield for growth, $\varphi_{\mu max}$, is taken equal to 0.06 mol C (mol quanta absorbed)$^{-1}$ according to converging analyses (BANNISTER and WEIDEMANN, 1984; DUBINSKY, BERMAN and SCHANZ, 1984; WELSCHMEYER and LORENZEN, 1981). The value assigned to $\varphi_{\mu max}$ linearly modulates the results of the computations.

Concerning the choice of $PUR_{1/2}$ a value of about 40 10^{-6} Usable Einst $m^{-2}s^{-1}$ is suggested by the experiments carried out at 19°C with a diatom, as reported in MOREL *et al.* (1987). KIEFER and MITCHELL (1983) adopted a value of ca. 115 10^{-6} Available Einst $m^{-2}s^{-1}$. According to the dominant colour of the submarine light field, such a value would correspond to 35 or to 70 10^{-6} Usable Einstein $m^{-2}s^{-1}$. It must be acknowledged that this physiological parameter is far from being well documented, particularly for natural populations. With $PUR_{1/2} = 40\ 10^{-6}$ Usable Einst $m^{-2}s^{-1}$ and equation 21b, the resulting P^B_{max} values can be computed in the various cases (Table 1). Obviously they are linearly related to the $PUR_{1/2}$ value adopted.

These P^B_{max} values are in the range of the most frequently observed values in temperate seas (KIRK, 1983). For all yield-irradiance relationships, the initial slope α' (equation 22c) takes the same value 23.76gC $(gChl\ a)^{-1}$ (Usable Einst $m^{-2})^{-1}$. When recalling that α' (MOREL *et al.*, 1987) can be between 1.5 and 3 times greater than α, the commonly defined slope, (i.e. defined with respect to Available Einstein) , the above figure falls within the range of the generally accepted values (see e.g. PLATT *et al.*, 1980; KIRK, 1983; YODER *et al.*, 1985).

The effect of temperature upon growth rate remains controversial. It is widely admitted that the light-limited regime and the initial slope are not affected by temperature, whereas P^B_{max}, the saturated value controlled by enzymatic dark reactions, is temperature dependent. Clearly shown *in vitro*, when acclimatized algae grown in culture are transferred to different temperature conditions (STEEMANN-NIELSEN and JORGENSEN, 1968), this effect could be less systematic in the natural environment because of possible adaptation or more likely selection (YENTSCH, 1974; KIRK, 1983). Tentatively, a van't Hoff dependency has been adopted, characterized by a Q_{10} (proportionate increase in growth rate per 10°C rise) equal to 1.88 as in EPPLEY (1972). This is simply introduced by allowing KPUR to become temperature-dependent according to:

$$KPUR\ (T) = KPUR\ (20°)\ 1.065^{(T-20°)} \qquad (29)$$

where KPUR (20°) is one of the values listed in Table 1.

5. RESULTS

5.1. *Sensitivity to the yield-irradiance parameterisation*

The functional dependence of the quantum yield for growth vis a vis PUR has been expressed through four different equations (23 to 26). Before undertaking any systematic use of the model

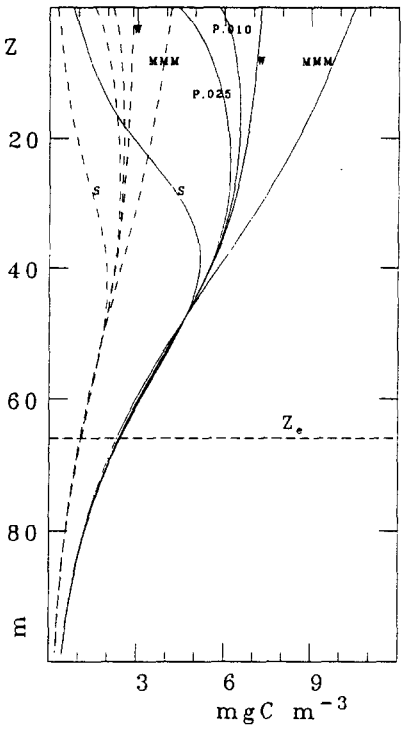

FIG. 7. Production profiles for two latitudes, for the vernal equinox and for a uniform chlorophyll profile (0.3mg m^{-3}, from 0 to 100 m). The various curves are for different yield-irradiance functions (see Tables 2 and 3; abbreviations are as in Fig 5). The solid and dashed curves are for the Tropic of Cancer and for 60°N, with temperatures of 20°C and 5°C, respectively. Abbreviations are as in Fig. 5.

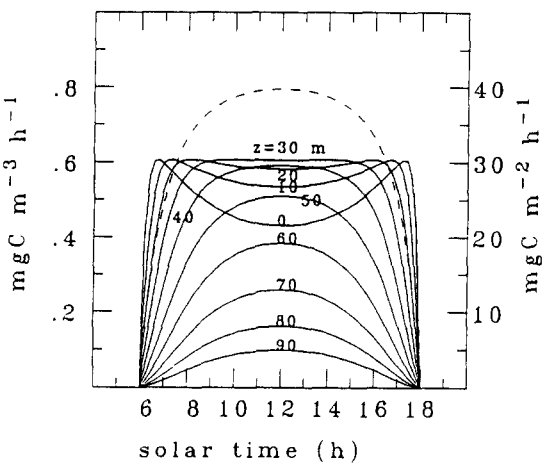

FIG. 8. Diurnal march of the production (mg C $m^{-3}h^{-1}$, left ordinate scale) at different depths (m), for the vernal equinox at the Tropic of Cancer. Computations are made by using equation 26 (with β = 0.01) and under the conditions adopted for the "standard run" (Table 2). The dashed curve represents the diurnal march of the depth integrated production (mg C $m^{-2}h^{-1}$, right ordinate scale).

TABLE 2. Values assigned to input parameters in the sensitivity studies dealing with the effect of the various yield-irradiance parameterisations, f(x)

Day	March, 21
Latitude	23°27' and 60° N
Sea temperature (uniform vertical profile)	20°C and 5°C
Atmospheric conditions	water vapor 2 cm, 0^3: 350 DU, V: 23 Km
	wind speed: 4 ms^{-1}
Vertically uniform chlorophyll profile with Chl = 0.3 mg m^{-3}	
(resulting in Z_e = 65.9 m at noon and $\langle Chl \rangle_{TOT}$ = 19.77 mg m^{-2})	
Physiological parameters	a^*_{max} = 33 m^2 (g Chl)$^{-1}$
	$\varphi_{\mu max}$ = 0.06 mol C/mol quanta absorbed
	$PUR_{1/2}$ = 40 µE $m^{-2}s^{-1}$

it is necessary to study the impact of these various expressions upon the results, and possibly to select one of them to define a standard run.

The tests are effected by running the model with the various f(x) functions and keeping constant all other involved parameters with the assigned values indicated in Table 2. When fixed, the physiological parameters lead to equal initial slopes of the production-irradiance curve, whatever the f(x) function, but lead to saturated P^B_{max} values which differ according to equation 22b.

The primary production profiles produced by the model with the various parameterisations are shown in Fig. 7; depth-integrated daily productions P and Chl-cross sections for photosynthesis ψ^* are displayed in Table 3. The diurnal march of the production at different depths for one selected example (Tropic of Cancer, vernal equinox) is also shown in Fig. 8.

The two formulations which do not account for inhibition lead to rather different profiles. With the MMM expression, local productions which continuously increase toward the top layer follow a profile which appears somewhat unrealistic. Saturated values in the upper layer could be obtained only under the proviso that $PUR_{1/2}$ be severely reduced, but that is incompatible with physiological data. In other circumstances, not shown here, this formulation systematically produces uncomfortably high ψ^* values.

The parameterisation making use of the Webb's formula provides a more realistic profile with steadily saturated P values in the upper layer. However, formulations which include the inhibition effect are certainly more advisable as the presently abundant results (*in situ* production or P vs I experiments) tend to prove that inhibition is a general phenomenon.

In the frame of Steele's formulation, the non-adjustable inhibition appears too pronounced. The inhibited production zone (overlapping almost half of the euphotic layer) could be moved upward and limited to the very upper layer by changing (i.e. increasing) $PUR_{1/2}$. Such an increase, a priori not defendable, would also provoke a correlative increase in P^B_{max}. Finally the parameterisation using Platt's formula produces acceptable figures for P and ψ^* as well as for the vertical profiles. It is worth noting that inhibition is also made temperature dependent by virtue of equation 29 which allows KPUR to vary. This link could be relaxed by changing accordingly

TABLE 3. Results of the sensitivity studies vis-a-vis the yield-irradiance function, f(x), used in simulations. P is the daily column production integrated between 0 and Z_e or, for the numbers between parentheses, integrated between 0 and 1.5 Z_e, ψ^* is the Chl-specific cross section for photosynthesis (between 0 and Z_e). The day is that of the vernal equinox

	23°27' N, T=20° C		60° N, T=5°C	
Types *	P gC m^{-2} d^{-1}	ψ^* m^2 (g Chl)$^{-1}$	P gC m^{-2} d^{-1}	ψ^* m^2 (g Chl)$^{-1}$
MMM	0.438 (0.477)	0.0754	0.181 (0.199)	0.0653
S	0.233 (0.263)	0.0384	0.086 (0.104)	0.0297
W	0.369 (0.409)	0.0635	0.150 (0.169)	0.0541
P.010	0.353 (0.393)	0.0608	0.142 (0.161)	0.0512
P.025	0.335 (0.374)	0.0576	0.133 (0.151)	0.0479

*Abbreviations are as in Table 1; P.010 and P.025 are for Platt formulation with $\beta = 0.01$ or 0.025.

the ß parameter in Platt's equation. It is, however, believed that this numerical correlation is naturally occurring. If at lower temperature, P^B_{max} (beside being depressed) occurs at lower irradiance, there are good reasons to think that the onset of inhibition will follow the same trend. Accordingly ß, once chosen, is kept constant regardless of the temperature.

With respect to those of Table 2, other case studies have also been effected by changing date, location and chlorophyll content. They essentially teach nothing more than do the presented results. For what follows Platt's formula, with $\beta = 0.01$, is adopted. This equation together with the atmospheric conditions and physiological constants summarized in Table 2, constitutes what is hereafter referred to as the "standard run". The chlorophyll concentration of 0.3 mg m^3, adopted as a typical mean oceanic value (see Appendix 3), is used in further systematic studies.

5.2. *Net carbon fixation and chlorophyll* a *biomass*

In Case I waters, only algae, together with their breakdown products, determine the depth of the euphotic layer as well as the spectral composition of the penetrating radiations, i.e. both optical properties of the water body which in turn govern the primary production. In view of understanding the basic phenomena, the following study is carried out under the simplifying assumption that chlorophyll is uniformly distributed along the vertical

$$\text{Chl}\ (Z) = \text{constant} = \overline{\text{Chl}}$$

and by allowing $\overline{\text{Chl}}$ to vary from 0.01 up to 20 mg m^{-3}. The depth of the euphotic layer, Z_e, which varies with changing $\overline{\text{Chl}}$, is displayed in Fig. 9. The computations made for noon, with a sun at Zenith (Equator, March 21) or when the sun has a low elevation (6°33', at 60°N, March 21) demonstrate that Z_e is practically insensitive to the sun's elevation because of the diffuse character

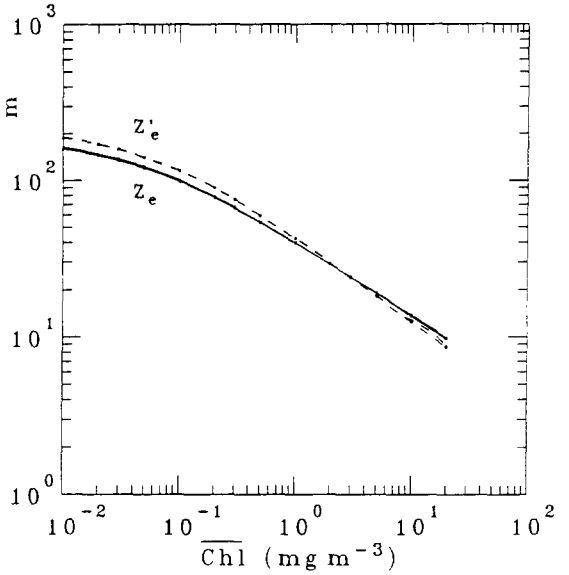

FIG. 9. Depth of the euphotic layer, Z_e, as function of the chlorophyll concentration within this layer (uniform profile). The dashed curve represents the depth, Z'_e, where subsists 1% of the photosynthetically usable radiation (PUR, see text). There are two Z_e and Z'_e curves (hardly distinguishable) for Equator and 60°N respectively at the vernal equinox.

of the in-water radiation field. Beside the conventional Z_e depth (defined with respect to available downwelling irradiance), another depth Z'_e, computed with respect to usable scalar irradiance (equation 21b), is also shown in Fig. 9 and will be discussed later.

The product $Z_e \overline{Chl} = \langle Chl \rangle_{TOT}$ is plotted vs $\overline{Chl}$ in Fig. 10. For the $\overline{Chl}$ range envisaged here, spanning 3.3 orders of magnitude, $\langle Chl \rangle_{TOT}$ is restrained to vary only within 2 orders of magnitude, between 2 and 200 mg m^{-2}, approximately. From a statistical analysis performed on field data which was presented elsewhere (precisely from equations 1 and 3 in MOREL, 1988) it follows that:

$$\langle Chl \rangle_{TOT} = 38\ \overline{Chl}^{0.572} \tag{30}$$

represented as the straight line in Fig. 10, which nicely agrees with the modelled values; (the curvature at low $\overline{Chl}$ is an effect of absorption by the water itself, which forces Z_e to take a finite value when $\overline{Chl}$ tends toward 0; thus the curve depicts the actual situation more realistically than does the empirical straight line).

The daily absorbed radiation by algae, ARA (equation 9), once normalized with respect to incident radiation just above the surface, is plotted as a function of $\overline{Chl}$ (Fig. 11a). The proportion of incident, photosynthetic energy, which is absorbed by phytoplankton within the euphotic layer, ranges from 0.6 to 70% according to the trophic state envisaged and would tend asymptotically toward 100% at very high $\overline{Chl}$ concentrations. The results are for the Tropic of Cancer and for the solstices; they may vary slightly according to the spectral composition of the radiation impinging at the surface, as analysed below.

At first sight, the absorbed-to-incident energy ratio is directly proportional to the depth-integrated biomass as shown in Fig. 11b; nuances do however exist. In reference to equation 10, the variations of the bulk cross section for absorption per unit of chlorophyll, A^*, can be illustrated

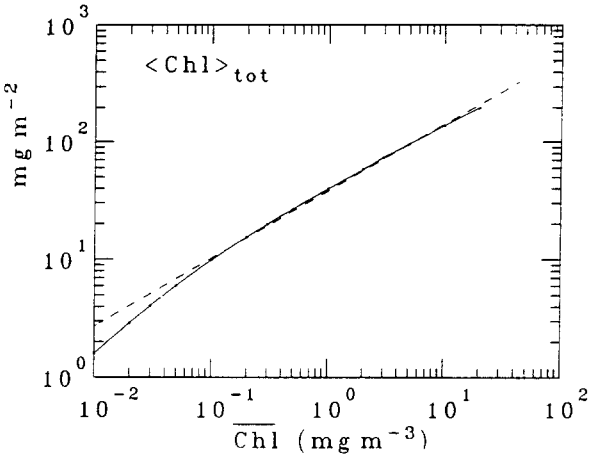

FIG. 10. Depth integrated (from 0 to Z_e) chlorophyll content $<Chl>_{TOT}$ as a function of the mean chlorophyll concentration within the euphotic layer. The straight line corresponds to equation 30.

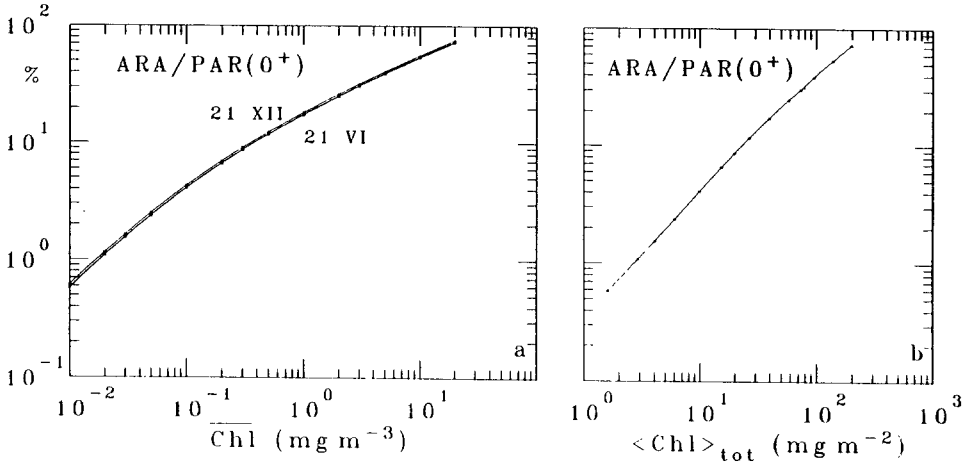

FIG. 11. Absorbed radiation by algae within the euphotic layer, ARA, normalized with respect to photosynthetic incident radiation above the surface, PAR (0^+), as a function of mean $\overline{Chl}$ concentration (panel a) or column integrated chlorophyll (panel b).

by forming the ratio $(ARA/PAR(0^+))/<Chl>_{TOT}$. The A^* values computed for various $\overline{Chl}$ concentrations are displayed on Fig. 12; the different curves correspond to various days and latitudes, i.e. to various spectral composition of the incident radiation. For a given day and location, A^* experiences, in the 0.4-1 mg. Chl m^{-3} range, a maximum which exceeds by 25% the lower A^* values obtained at high or low chlorophyll concentrations. On the one hand, the residual green light in eutrophic waters is not amenable to an efficient absorption by algae. On the other hand, in oligotrophic waters, where blue light is more efficiently absorbed by blue absorbing pigments, water competes with algae in capturing energy within thickening euphotic layers. Therefore the most favourable situation with respect to absorption by algae is that of mesotrophic waters, as reflected by the maximum in all A^* curves.

The bulk absorption cross section also depends on the spectral composition prevailing at the

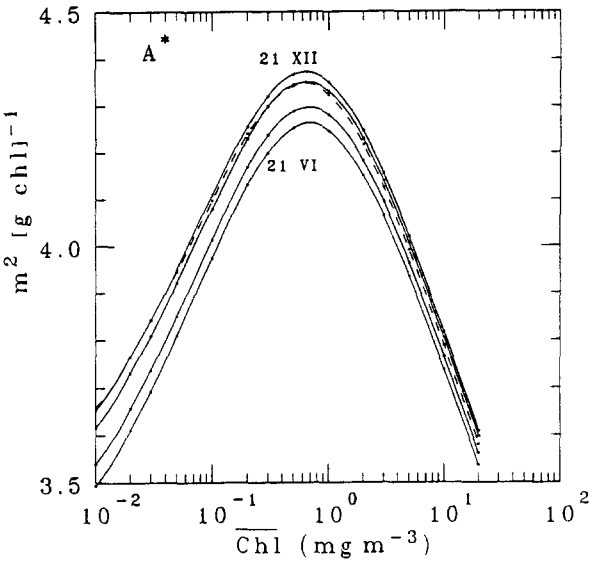

FIG. 12. Bulk absorption cross section by unit of chlorophyll, A* (see equation 10) computed for the entire day and the entire euphotic layer as a function of the mean chlorophyll concentration. Solid curves are for the Tropic of Cancer, and from bottom to top, for June 21, March 21, February 7 and December 21. The dashed curve is for 60°N and for the winter solstice.

surface which is governed by the sun altitude. This is shown by the translation which affects the A* curves when the date is changed. An increase in A* by approximately 15% is observed between the summer solstice at the Tropic of Cancer and the winter solstice at 60°N (the sun elevation at noon being respectively 90° and 6°33'). The increasing and blueing sky radiation when the sun has a low elevation (see Fig.1) is the cause of this trend.

The net primary production (P) computed for the entire (homogeneous) euphotic layer is shown as a function of the thickness of this layer in Fig. 13. The situations represented are for the two solstices and for the Tropic of Cancer (the temperature is assumed to be constant, 20°C in both seasons). The computed values are well in the range of commonly observed values. Their variations with Z_e closely follow those of the integrated biomass (the curve which shows the relationship between $<Chl>_{TOT}$ and Z_e is drawn on the same figure for comparison). All the P values, whatever the depth Z_e or the chlorophyll concentration, are increased by ca. 35% between the winter and the summer solstices, whereas the incoming energy is almost doubled at this latitude with PAR(0^+) varying from 6.88 to 12.85 MJ $m^{-2}d^{-1}$. As stated above, higher sun and higher radiative energy, provoke a diminishing in the absorption capacity of the euphotic layer (in A*). However, for the dates considered A* is only depressed by 5% which is thus insufficient to explain the non linear trend of P with respect to PAR(0^+). The change in the yield attached to the transformation of absorbed energy into chemically stored energy is the main factor to be invoked.

This is made clear in Fig. 14 where the number Φ^* (equation 11), which, in a dimensionless way expresses this yield, is plotted as a function of $\overline{Chl}$ for the two dates in question, and some other intermediate ones. The relative position of the curves demonstrates that Φ^*, whatever the trophic state, is depressed by about 25% when incident irradiance increases from its minimal value (21st December) to its maximal value (21st June). This overall decrease is obviously related to the fact that algal photosynthesis is realised more efficiently at low radiative level. It is worth

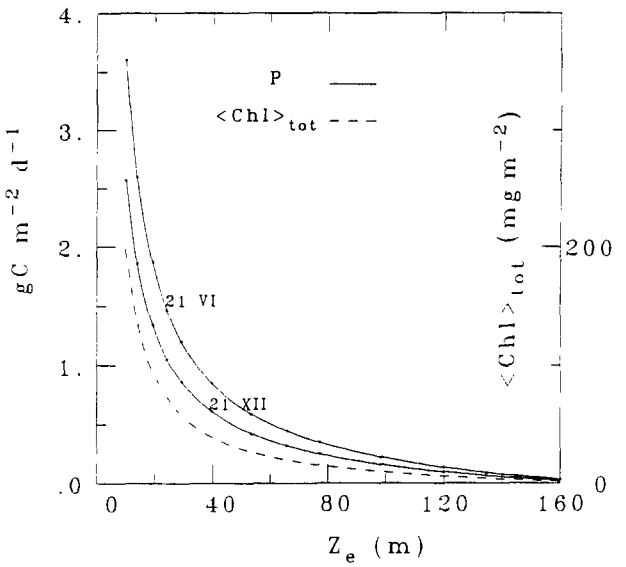

FIG. 13. Net primary production P per day and m^2 as a function of the depth of the euphotic layer Z_e. Latitude is that of the Tropic of Cancer; the two solid curves are for the two solstices. The dashed curve represents $<Chl>_{TOT}$, as a function of Z_e (right ordinate scale).

recalling that this general pattern is partly dependent on the choice of the f(x) function; therefore the computed decrease (in the frame of Platt's formulation with ß=0.01) can only be considered to be a reasonable tentative estimate.

Given the day and latitude, or in other words given the amount of radiant energy, the global yield Φ^* is maximum at low chlorophyll content, it then undergoes a minimum (for $\overline{Chl}$ ~ 2mg m^{-3}) before gently increasing at higher $\overline{Chl}$ concentrations. The extreme values in this graph (2.1 and 1.4%), when converted into φ_μ (eq. 13a) by using the appropriate factor (1/1.943), lead to mean quantum yield values for growth ranging from 0.01 to 0.007 mol C/mol available photons, for the whole day and the entire euphotic layer.

The Chl-cross section for photosynthesis ψ^* (equations 1 and 11) is shown in Fig. 15, for the same location, dates and chlorophyll range as used in Fig. 14. These ψ^* values, from 0.055 to 0.080m^2 $(g.Chl)^{-1}$, fall within the range of observed values for this "bio-geochemical constant". It is interesting to note that ψ^* is unexpectedly quasi-independent from the trophic state, as long as $\overline{Chl}$ is lower than 1mg m^{-3}, and only slightly decreases when waters become eutrophic. Such constancy supports the interest given to this parameter. Indeed, ψ^* is much more sensitive to the surface light conditions than to the photosynthetic pigment concentration. For instance, a change of ±0.01 $m^2(g\,Chl)^{-1}$ is observed at 23°27'N, the latitude considered, according to the season. Such a sensitivity to the radiative level suggests that ψ^* can be greatly modified by cloudiness. The magnitude of this effect will be examined later.

It is difficult at this stage to ignore the effect of temperature. The relative increase of ψ^* induced by a lower radiation availability in high latitudes, is expected to be drastic, as confirmed by numerical simulations. In the natural environment, it is likely counterbalanced by the depression of the photosynthesis process resulting from lower temperatures. If ψ^* is computed at 60°N, uncomfortably high values appear (~ 0.14$m^2(gChl)^{-1}$ and even 0.60 for the shortest days), so long as a temperature-controlled growth is not considered. By assuming a temperature of 5°C

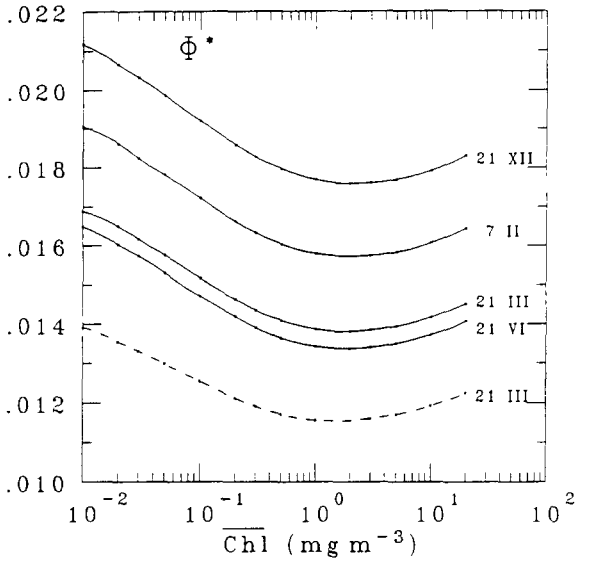

FIG. 14. Dimensionless yield Φ * (equation 11) of the energy storage through net photosynthesis, as a function of the mean chlorophyll concentration, for different dates, as indicated, and for the Tropic of Cancer. The dashed curve is for the vernal equinox at 60°N with a temperature of 5°C.

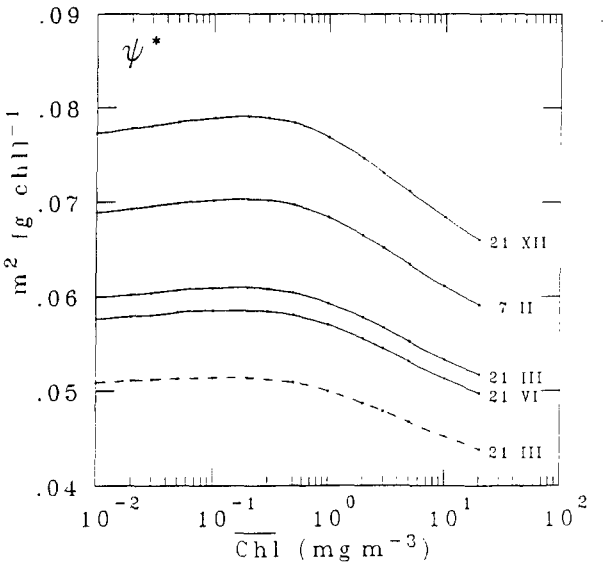

FIG. 15. Chlorophyll-cross section for net photosynthesis, ψ * (equation 1), as a function of the mean Chl concentration, for the Tropic of Cancer or for 60°N, and various dates as indicated (solid curves); the dashed curve is for 60°N with a temperature of 5°C.

and using the Eppley dependence (equation 29), ψ* is reset to normal values (dashed curve in Fig.15). In the following section, the temporal and zonal variability of primary production will be established under the proviso expressed by equation 29 and by using climatological values for the sea surface temperature.

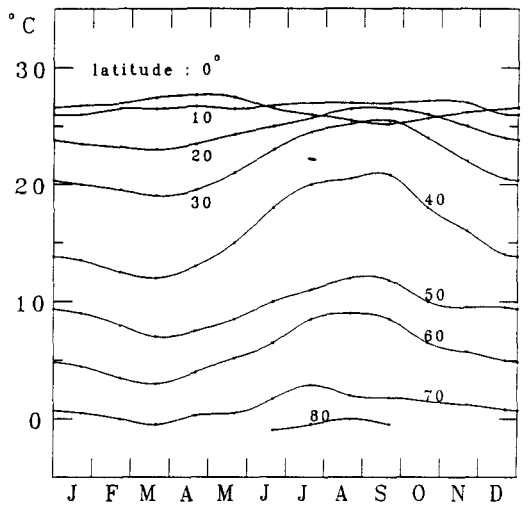

FIG. 16. Annual march of sea surface temperature for various latitudes (0 to 80°) in the North Atlantic Ocean, according to Bohnecke, cited in NEUMANN and PIERSON (1966).

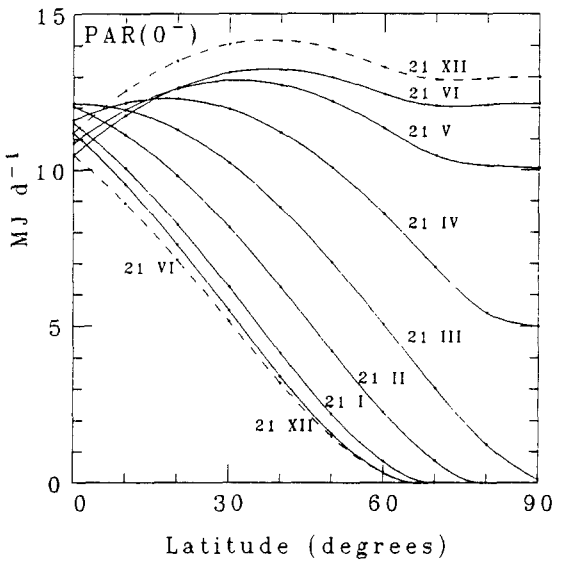

FIG. 17. Photosynthetic available radiation, PAR (0^-), computed below the surface with a wind speed of 4m s^{-1}, shown as a function of latitude and season and for clear skies. The dotted curves are for the southern hemisphere and for the two solstices only.

5.3. *Temporal and zonal variability of primary production and related parameters*

For the purpose of such a geographical study, the annual change of sea surface temperature, for the zonal mean at different latitudes, has been taken from NEUMANN and PIERSON (1966). These data, established for the North Atlantic Ocean (by Böhnecke) are graphically presented in Fig. 16. The photosynthetic available irradiance below the surface PAR(0^-),computed for clear skies and as a function of latitude and season, is shown in Fig. 17.

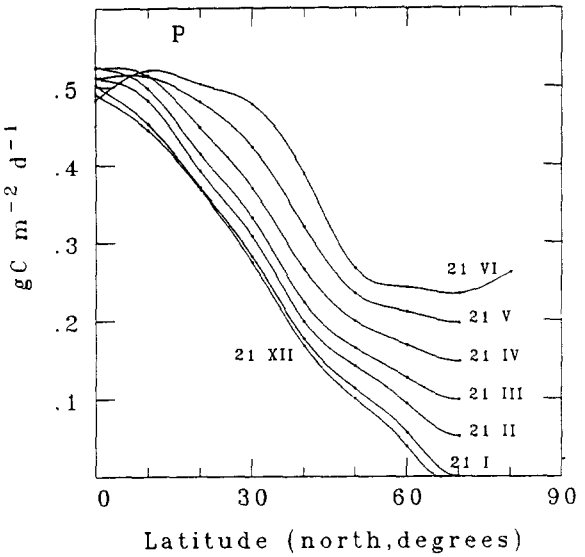

FIG. 18. Net primary production within the euphotic layer as a function of latitude and season and for clear skies. Uniform vertical profiles are assumed with $\overline{Chl} = 0.3$ mg m^{-3}.

A constant value of 0.3 mg m^{-3} is assigned to the chlorophyll concentration within the productive column in all the following computations. The corresponding primary productions are displayed in Fig. 18. As expected, the values at the equator, which are of the order of 0.5 gC m^{-2}d^{-1}, remain almost constant all year round, whereas the seasonality increases with increasing latitude. At the mid-latitude, for instance, a twofold change in P occurs between the winter and summer solstices. In the polar zones, the production starts from zero after the winter period and then increases in the summer time, up to a value approximately half of that at the equator. At these latitudes, the radiation energy at the sea surface is comparable to, or even exceeds, that experienced at the equatorial belt. The depressive effect of low temperature (within a factor 4.8 for a temperature difference of 25°C) is partly compensated by the improved conditions for photosynthesis which result from relatively low illumination associated with long (24h) exposure. The global yield Φ^* is approximately doubled in response to these favourable light conditions. The general trend exhibited by the curves in Fig. 18 seems to be plausible; it is recognised, however, that precise numbers cannot be produced as long as some important physiological parameters remain inadequately described.

Using the same parameter values as for Fig. 18, the ψ^* estimates produced by the model are shown in Fig. 19. Disregarding some very high values discussed below, the majority of ψ^* values lie within the range 0.04 - 0.10 m^2(g Chl)$^{-1}$, overlapping experimental values obtained in the field. At a given latitude, ψ^* tends to decrease from the winter to the summer season, the changes between equinox and summer solstice are limited, compared to those during the first quarter of the year. The span of the ψ^* values is wider for high latitudes, as is the span of the radiation influx (Fig.17). The lowest values, observed at high latitude in summer, result from the low temperature effect already discussed, but perhaps exaggerated. The highest ψ^* values in Fig. 19 are probably just anecdotal; they all occur in high latitudes during the shortest days and at vanishing irradiations (<0.5 MJ m^{-2}d^{-1}) leading to insignificant production. When the daily time course of production is examined in detail, similar anomalously high yields are also momentarily obtained everywhere during dawn and dusk.

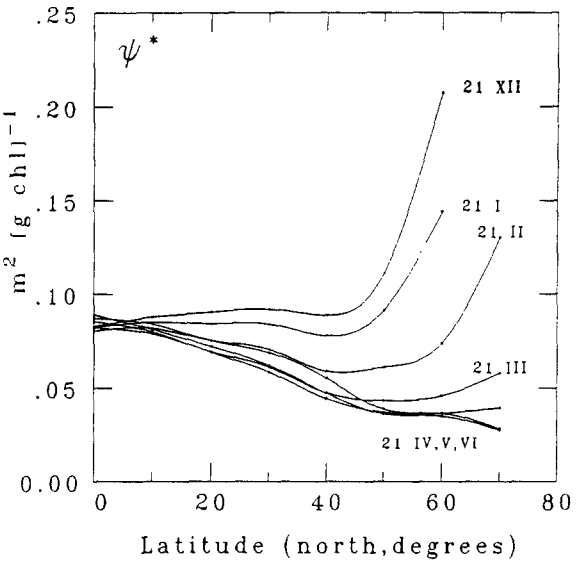

FIG. 19. Chlorophyll cross section for net photosynthesis, ψ^*, with the same conditions as for Fig. 18.

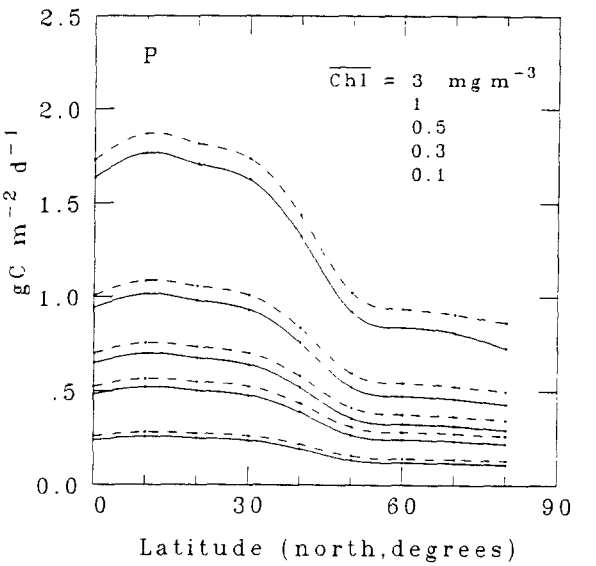

FIG. 20. Net primary production for different mean chlorophyll concentrations (values in the same order as the curves), plotted as function of latitude for the summer solstice. The solid curves are for production within the euphotic layer (0 to Z_e), the dashed curves for the layer extending from 0 to $1.5Z_e$.

A set of figures like Figs 18 and 19 could be produced for chlorophyll concentrations other than 0.3mg m^{-3}. However, the trends are predictable at least for a first approximation. This approximation is based on the results of Fig. 15 which demonstrate that ψ^* is essentially constant with respect to $\overline{Chl}$ and over a wide range for this parameter. Therefore, the values plotted in Fig. 19 will remain practically unchanged whatever the $\overline{Chl}$ concentration (except if very high). By virtue of equation 1 and with ψ^* admittedly independent from $\overline{Chl}$, deriving values of PSR or P

TABLE 4a. Relative importance of production in deep layers (below Ze) with uniform chlorophyll profiles

Chl (mg m^{-3}) =	0.03		20	
	$\Delta P/P(Z_e)$	$\Delta\psi^*/\psi^*(Z_e)$	$\Delta P/P(Z_e)$	$\Delta\psi^*/\psi^*(Z_e)$
high sun (vernal equinox at equator, daylength 12 h)	+12.3%	-25%	+6.5%	-29%
low sun (winter solstice at 60• N, daylength 5.5 h)	+2.8%	-31%	+1.3%	-32.5%

in Fig. 18 would be simply achieved by multiplying by the new value of $\langle Chl \rangle_{TOT}$, when $\overline{Chl}$ is varied. Exact computations were carried out running the model for diverse $\overline{Chl}$ values; but only the results for the summer solstice are presented (Fig.20).

5.4. *Primary production below the so-called euphotic depth, Z_e*

For all the above reported simulations, the uniform chlorophyll profile was extended below Z_e and computations were carried out down to a depth $D = 1.5\ Z_e$. There are reasons to expect that net carbon fixation within these deeper layers may be non-negligible, as often experimentally detected. Disregarding the possible adaptation of some algae at very low light level and considering only the physical aspects, at least three main reasons can be invoked:

(i) the light-limited regime is controlled by the absolute, rather than by the relative values of radiant energy,

(ii) the arbitrary character of the "1% level" is reinforced by the fact that its definition involves downwelling, instead of scalar, irradiance (cf. Appendix 1),

(iii)the capacity of algae in harvesting light is not a constant throughout the spectrum, so that the spectral quality of the remnant radiations is as important as its amount.

Evidence of these effects is presented when the depth Z'_e is computed and compared to the conventional Z_e in Fig. 9; Z'_e is the depth where the scalar irradiance, once converted into usable radiation, is reduced to 1% of the PUR value computed above the surface (with in this case the downwelling E_d irradiance - see Appendix 1). As expected, Z'_e exceeds Z_e in low-chlorophyll, blue waters by more than 20m when Z_e>100m. At Z_e, in effect, more than 2 or 3% of usable radiation is still present. On the contrary, in green waters when $\overline{Chl}$>3mg m^{-3}, Z'_e can become smaller than Z_e.

The consequences of these effects on deep production can be established since the model ignores the drawbacks included in the definition of Z_e. Only two extreme cases are given in Table 4a. The deep production, ΔP, within the layer extending from Z_e to $1.5\ Z_e$ represents 12.3% of the production within the conventional euphotic layer, denoted $P(0, Z_e)$, in the most favourable situation (blue water, high solar energy), but only 1% in the least favourable situation (green water, low solar energy).

The depth of integration for both column production and areal chlorophyll directly affects the computation of ψ^*. With a uniform profile extended to $1.5Z_e$, the integrated chlorophyll is multiplied by 1.5. If the production beyond Z_e is practically insignificant, ψ^* is obviously reduced by 33%. This situation is observed in green, weakly lit waters (Table 4a). Noticeable deep production can partly counterbalance this reduction, nevertheless ψ^* remains reduced by 25%.

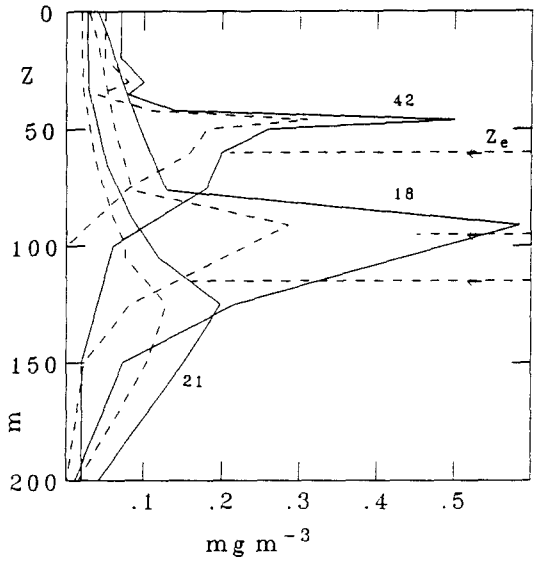

FIG. 21. Vertical profiles of Chl *a* + Pheo *a* concentration (solid lines) or of Chl *a* only (dashed lines), at Station 21 and 18, Discoverer cruise (TYLER, 1973) and at Station 42, Guidom cruise (GROUPE MEDIPROD, 1977). The arrows indicate the measured euphotic depth Z_e.

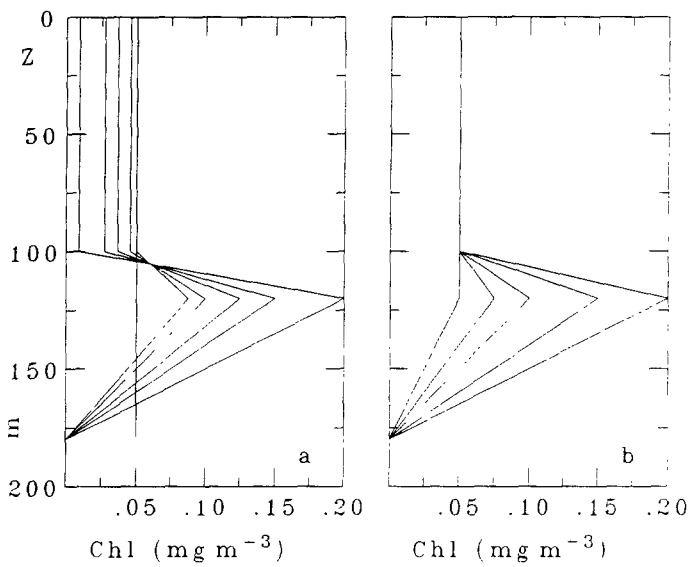

FIG. 22. Idealized vertical chlorophyll profiles used in simulations. In panel a the integrated column (from 0 to 180 m) is constant (9 mg m^{-2}). In panel b the concentration within the upper layer (0-100 m) is constant (0.05 mg m^{-3}), whereas the deep maximum is varying.

even when ΔP is maximal (blue waters, high sun). This pitfall, of methodological order, has been astutely identified by CAMPBELL and O'REILLY (1988) as being a plausible cause for the difference between reported ψ values in recent literature.

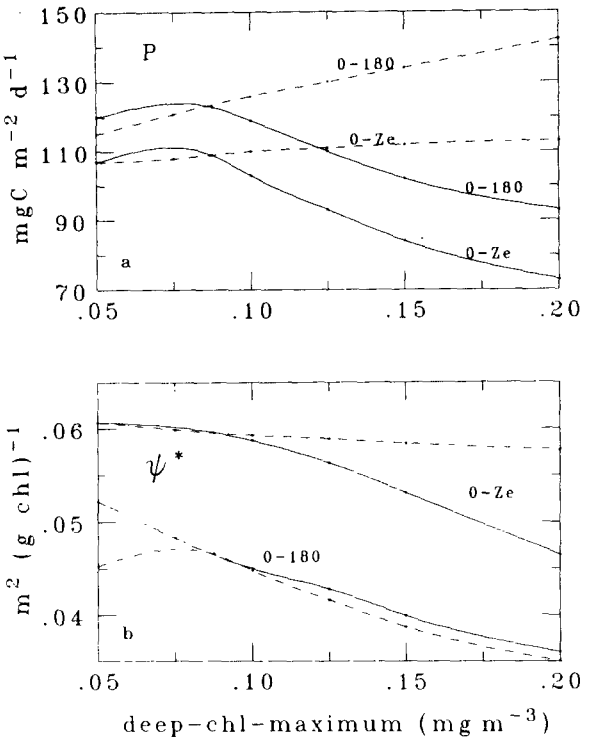

FIG. 23. As a function of the peak value in the deep Chl maximum, are shown the production (a) and in (b) the parameter ψ *. The solid curves are for the idealized profiles of Fig.22, panel a, the dashed curve for profiles in panel b. P and ψ * are given for the layer (0,180m) or for the euphotic zone (0,Z_e) as indicated.

5.5. *Production in a deep chlorophyll-maximum layer*

A common feature in stratified oligotrophic tropical waters is the development of a well defined chlorophyll maximum near the bottom of the euphotic zone (see historical references in JAMART *et al.*, 1977). The hypothesis of uniformity, as adopted above, fails in many occasions and the contribution of deep layers to production can be higher than the ΔP values given in Table 4a. It is beyond the scope of the present study to analyse this effect in all its aspects (a thorough analysis exists in PLATT, SATHYENDRANATH, CAVERHILL and LEWIS, 1988; SATHYENDRANATH, PLATT, CAVERHILL, WARNOCK and LEWIS, 1989). The present objective is restricted to examine if such a feature induces significant changes in P and in ψ*.

Typical profiles are shown in Fig. 21. They exhibit an assymetrical pattern with a sharp increase in Chl concentration resulting in a maximum close to Z_e, and then followed by a progressive decrease, down to a depth close to $1.5Z_e$. The shapes of these profiles are coarsely simulated (Fig. 22a) under several constraints as follows:(i) uniform profile above the Chl-maximum layer, (ii) maximum occurring at a fixed depth (that of Z_e in absence of maximum), (iii) Chl = 0 at the depth $1.5Z_e$, (iv) finally, the integrated Chlorophyll content from 0 to $1.5Z_e$ is kept constant whatever the extension of the peak. In practice, a "reference" uniform profile is initially defined with $\overline{Chl}$ = 0.05mg m^{-3}, leading to Z_e = 119.9m and to a column (0,$1.5Z_e$) integrated chlorophyll of 9mg m^{-2}. The profiles which include a deep maximum are constructed

TABLE 4b. Relative importance of deep production, with non uniform chlorophyll profiles, but constant integrated chlorophyll content (over a layer 0,180 m, cf. Fig. 22a.)
Conditions: Vernal equinox, tropic of Cancer

		Deep chlorophyll values (mg m^{-3})		
		0.05 (no peak)	0.10	0.20
Chl concentration in upper layer	mg Chl m^{-3}	0.050	0.0455	0.0091
Z_e	m	119.8	119.9	133.0
Z'_e	m	140.1	138.4	149.8
$<Chl>_{0,Ze}$	mg Chl m^{-2}	6.00	5.98	5.34
$<Chl>_{0,180}$	mg Chl m^{-2}	9	9	9
$P(0,Z_e)$	mg C m^{-2} d^{-1}	107	103	73
P (0,180)	mg C m^{-2} d^{-1}	120	119	93
$\Delta P/P\ (0,Z_e)$	%	12.1	15.5	27.4
$\psi^*(0,Z_e)$	m^2 (g Chl)$^{-1}$	0.0607	0.0587	0.0465
$\psi^*(0,180)$	m^2 (g Chl)$^{-1}$	0.0453	0.0448	0.0350

TABLE 4c. Relative importance of deep production with non uniform profiles constructed with a varying superimposed maximum (cf. Fig. 22b)
Conditions: Vernal equinox, tropic of Cancer

		Deep chlorophyll — maximum values (mg^{-3})		
		0.05 (no peak)	0.10	0.20
Chl concentration in upper layers	mg Chl m^{-3}	0.05	0.05	0.05
Z_e	m	119.8	117.7	115.5
Z'_e	m	140.1	136.0	129.9
$<Chl>_{0,Ze}$	mg Chl m^{-2}	6.0	6.28	6.67
$<Chl>_{0,180}$	mg Chl m^{-2}	7.5	9.75	13.50
$P(0,Z_e)$	mg C m^{-2} d^{-1}	107	110	113
P (0,180)	mg C m^{-2} d^{-1}	115	126	142
$\Delta P/P\ (0,Z_e)$	%	7.5	14.5	25.7
$\psi^*\ (0,Z_e)$	m^2 (gChl)$^{-1}$	0.0607	0.0593	0.0577
$\psi^*(0,180)$	m^2 (g Chl)$^{-1}$	0.0522	0.0450	0.0360

with a constant value from 0 to 100m, a linear increase from 100 to 120m (variable peak value) and then a linear decrease with Chl = 0 at 180m. With these profiles as input, the model is run for the Tropic of Cancer and vernal equinox. The results are graphically presented as a function of the peak value (Fig. 23).

The relative importance of the deep production, depicted as above by $\Delta P/P\ (0,Z_e)$, is 12%, in the absence of a maximum (see also Table 4b). When the peak develops and reaches 0.2 mg m^{-3}, this number increases up to 27%. Meanwhile the Chl concentration in the upper layer drops from 0.05 to 0.009 mg m^{-3}, whereas Z_e departs from its initial value (120 m) to attain 133 m. Due to the diminishing biomass above Z_e, the integrated production (from 0 to Z_e) obviously declines, as well as the production computed for the entire (0 to 1.5 Z_e) zone (Fig. 23). The corresponding ψ^* parameters follow the same trend (Fig. 23b). In summary, under the constraint of a constant biomass (0 to 120 m), the development of a deep Chl-maximum with the subsequent impoverishment of the upper layers would have a detrimental effect on integrated production (and on ψ^*). Such a normalisation may be thought as leading to a fallacious conclusion.

Therefore an un-normalized method is also envisaged. It consists of creating a deep maximum without changing the concentration within the upper layer (0.05 mg m^{-3}, from 0 to 100 m) and by keeping Chl = 0 at 180 m (Fig. 22b). The total biomass (0,180 m) is now increased by 80% and the deep biomass (from Z_e to 180 m) is multiplied by a factor 5 when the peak value reaches 0.20 mg m^{-3}. The evolution of $\Delta P/P\ (0,Z_e)$ is similar to that obtained in the previous case (see Table 4c). As expected $P\ (0,Z_e)$ is practically constant, whereas P (0,180 m) increases by 26% (Fig. 23). Accordingly $\psi^*\ (0,Z_e)$ remains almost constant, but ψ^* (0,180 m) is reduced to 69% of its initial (no peak) value, when the peak reaches 0.2 mg m^{-3} (Fig. 23). In spite of the improved yields attached to low energy levels, the deep biomass is unable to enhance drastically the global production within the entire (1.5 Z_e) sunlit column, as sometimes proposed to account for the under-evaluation of the primary production in oligotrophic zones. An under-evaluation of about 20 or 30%, however, can result from neglecting this deep production which occurs below the conventional euphotic depth.

As a test of the validity of the above conclusions, the model has been applied with its standard physiological input parameters to the actual Chl profiles shown on Fig. 21. For the days and latitudes considered, the productions computed for the euphotic zone nicely agree with the actual values (which were measured under cloudless skies and within a quasi-homothermal layer). The computed values are 88, 132 and 154 mg C $m^{-2}d^{-1}$ for the *Discoverer* stations 21 and 18 and for the *Guidom* station 42, respectively, instead of 71, 143 and 142 mg C $m^{-2}d^{-1}$ according to the measurements (Tyler, 1973; Groupe Mediprod, 1977). In such simulations using actual profiles, the radiant energy is propagated by using the (chlorophyll + pheophytin) concentrations, whereas the production is computed on the basis of only "active" pigments (Chl *a* concentration).

5.6. *Influence of pheopigments upon production*

The bio-optical model used when propagating the downward irradiance depends upon the total pigments (Chl *a* + Pheo *a*) concentration (the algal index, denoted "C" in Morel, 1988) and not upon the sole Chl concentration. In effect, the discrimination between the optical influences of these two kinds of pigments was unachievable from field data. Equation 16, however, was formally written as if active chlorophyll was the only pigment present in the water column. Replacing (Chl) by (Chl + Pheo) in this equation does not modify the results for the depth Z_e as well as the spectral composition of the light field at various depths. This has a straightforward

consequence. With Z_e independent from ρ, with

$$\rho = (\text{Chl } a) / (\text{Chl } a + \text{Pheo } a)$$

the production will be linearly related to ρ, provided that ρ is constant with depth; ψ^* will remain unchanged because $<Chl>_{TOT}$ is also proportional to ρ. Prediction is not so simple if ρ is assumed to vary with depth. To imagine such an effect, computations have been effected by considering a uniform vertical profile in terms of (Chl *a* + Pheo *a*) concentration, with a value of 0.3 mg m^{-3} (leading to Z_e=65.9 m) and very contrasting, purely hypothetical situations as follows (i) ρ= 0.5 whatever the depth Z, (ii) ρ linearly decreasing from 1 at the surface to 0 at $Z=Z_e$, (iii) ρ linearly increasing from 0 to 1 for Z going from 0 to Z_e. Situations (ii) and (iii) lead to P and ψ^* respectively increased or decreased by 12.4% with respect to P computed for situation (i). Indeed, according to a statistical analysis (MOREL and BERTHON, 1989), the ρ-profiles appear to be essentially featureless.

The question can also be envisaged from another viewpoint, that of a given Chl *a* profile to which pheopigments are progressively added. In such situations the quantities Z_e, P and also $<Chl>_{TOT}$ are all progressively diminishing in a non-linear manner with regard to ρ. The sensitivity study howbeit shows that ψ^* remains constant within less than 1%, when ρ (constant with respect to depth) diminishes from 1 to 0.5.

5.7. *Production in the case of realistic biomass profiles*

From a statistical analysis of about 4000 stations in Oceanic case I waters, it has been shown that the vertical biomass profiles are not randomly shaped (MOREL and BERTHON, 1989). According to the trophic state (the pigment content within the euphotic layer), the profiles evolve

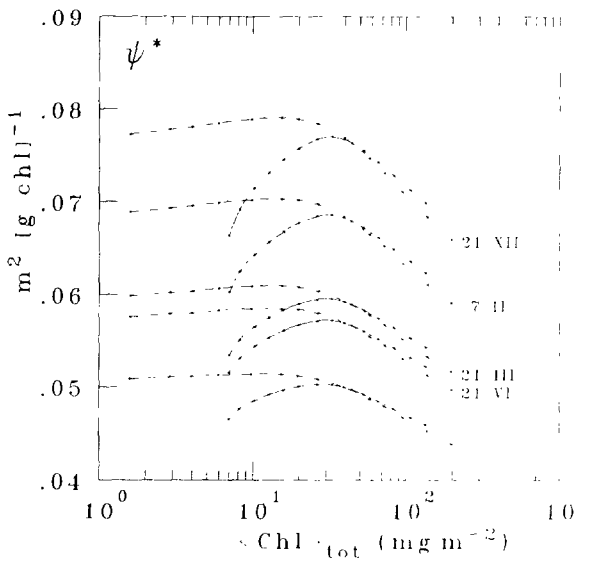

FIG. 24. The chlorophyll-cross section for net photosynthesis ψ^* as a function of the column $(0,Z_e)$ integrated pigment concentration, for the Tropic of Cancer for those dates indicated. The lower curves are for 60° N and for the 21st of March. The dashed curves are for biomass uniformly distributed along the vertical; the solid curves for non-uniform profiles (see text).

in a rather regular way, between oligotrophic waters exhibiting a well marked deep maximum, mesotrophic waters for which this maximum is progressively weakening and broadening and, finally, eutrophic waters, characterized by smooth, slightly decreasing (from 0 to Z_e) profiles.

This evolution (for stratified waters, as the deeply mixed waters in high latitude do not follow this pattern) can be parametrized (equation 6 in the above reference) as a function of the pigment content. These modelled profiles are generally representative of realistic situations and can be included in the production model. Thus the impact of actual vertical pigment distribution upon ψ^* can be examined.

The ψ^* values computed for these non-uniform profiles are shown in Fig. 24 as a function of the column integrated active chlorophyll (statistical ρ values are also taken into account). The $<Chl>_{TOT}$ range is restricted (7 to 150 mg Chl m^{-2}) to conform with the actual data used in the statistical analysis. For the sake of comparison, the ψ^* values for uniform profiles are also displayed (this is another presentation of the results already shown in Fig. 15). There is practically no difference between the two sets of ψ^* values when dealing with mesotrophic or eutrophic waters ($<Chl>_{TOT}$ > 30 mg Chl m^{-2}). In oligotrophic situations and for decreasing biomass, an increasing departure occurs, with ψ^* values progressively depressed as a consequence of the development of a deep maximum (as in Table 4b and 4c). The corresponding production values and profiles, for both uniform and non-uniform distributions, can be found in MOREL and BERTHON (1989).

In the perspective of interpreting the remotely sensed ocean colour data in terms of productivity, a consequence emerges with respect to the ψ^* values to be used. If a climatological (zonal, temporal) field of ψ^* is needed, this field has also to be diversified by considering as a supplementary variable the trophic state which determines the shape of the biomass profile. The above calculation is an illustration of such an approach.

5.8. *Influence of cloudiness upon production and ψ^**

The non-linear response of production to the radiative level and the subsequent changes in ψ^* have already been mentioned when dealing with clear skies (Figs 13 and 15). Cloudiness can severely reduce the incident energy at the surface with consequences upon the primary production which can be assessed through the use of the model.

At least for the visible part of the spectrum, a reasonable approximation consists of considering that cloudiness does not notably affect the spectral composition of the daylight which, in the absence of clouds, would result from the addition of direct and diffuse radiations. Under this approximation the simulation of diverse states of cloudiness is simple: it suffices to run the model as before, except that PUR (λ,Z,t) has to be modified, i.e. reduced, before entering into equation 21b (and then 27 and 28). The reduction is obtained by applying a factor, less than 1, which describes the global transmittance by the cloud cover. Equation 14 has also to be modified by equalising E_{sky} to E_{TOT}, that leads to $\mu_o(\lambda)$ = constant (this modification is numerically of minor importance). Cloud transmittance, t_c, is high for transparent cirrus, and is of the order of 0.4 - 0.6 for middle-level scattered clouds and can be as low as 0.2 for heavily overcast or foggy skies (see e.g. COULSON, 1975). This factor, t_c, is given values ranging from 1 to 0.1 in the following simulations, and the results are displayed in Fig. 25.

Productions computed under cloudy sky conditions are normalized with respect to production under a clear sky for the same day and location. The departure from linearity is spectacular. At the Tropic of Cancer and on the 21st June, the carbon fixation is depressed by 15% only, while

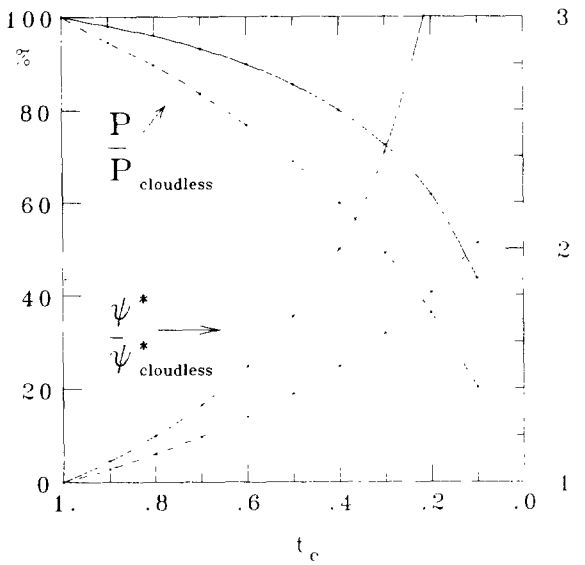

FIG. 25. As a function of t_c (= PAR (0^+) cloudy skies / PAR (0^+) cloudless sky), production, when normalized with respect to that occurring for a cloudless sky (at the same location and date; expressed as %, left ordinate scale). The corresponding ψ^* values, also normalized by ψ^* in cloudless conditions are also shown (right ordinate scale). The solid curves are for the summer solstice at the Tropic of Cancer and dashed curves for 60°N and the winter solstice.

cloudiness leads to a halving of the available energy. Even during very dark days ($t_c = 0.20$) a substantial production still occurs (half of the potential maximum). The Chl-cross section for photosynthesis is accordingly strongly enhanced (see solid curve in Fig. 25, where ψ^* is also normalized with respect to its minimal value for a cloudless day). It is, for instance, multiplied by 2 when cloud transmittance is 0.4. These patterns are neither perceptibly modified when changing the pigment content nor affected by date and latitude (except for vanishing irradiation, which already leads to anomalously high ψ^* values, cf. Fig. 19 and dashed curves in Fig. 25). It is interesting to note that measurements at *Discoverer* stations 10 and 12 were carried out at the same location (SE of Galapagos islands) with almost unchanged biomass but under different sky conditions, cloudy on the 14th and sunny on 16th May 1970. These measurements lead to ψ^* values (equal to $2.4\,\bar{\epsilon}/\langle Chl \rangle$ in MOREL, 1978) which increased by 46%, namely increasing from 0.073 to 0.106 m^2(g Chl a)$^{-1}$, when cloudiness reduced PAR (0^+) by 40% (TYLER, 1973). These observations agree with predictions in Fig. 25.

Some of the high ψ (or ψ^*) values reported in the literature are likely to have originated from such a cloudiness effect. Figures 8 and 10 in CAMPBELL and O'REILLY (1988) tend to support this conjecture. This effect has also to be kept in mind when looking at geographical results, such as those in Fig. 18, all established for clear sky conditions. In natural environments with sporadic and episodic cloudiness, the average ψ^* values are likely to be enhanced with respect to those of Fig. 18. Assuming a mean cloud transmittance of 0.5, which induces an increase in ψ^* by a factor 1.7 (Fig. 24), and a mean cloud coverage above the ocean of 0.43 (see e.g. LIOU, 1980), a time and space averaged factor applying to all climatological ψ^* values would be of the order of 1.30.

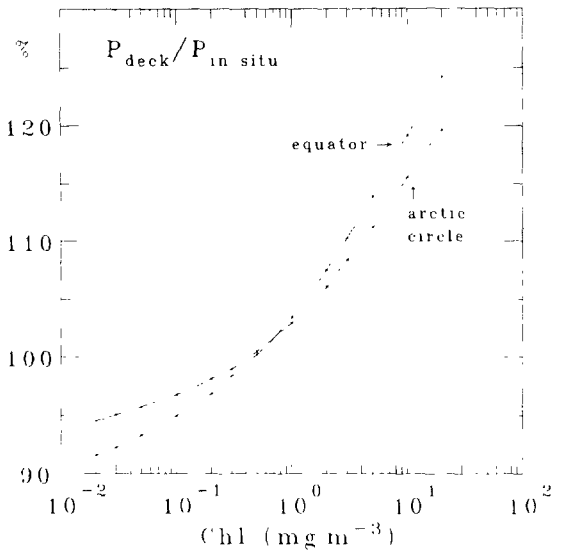

FIG. 26. Ratio of the deck incubation production values to *in situ* incubation production values, as a function of the chlorophyll concentration within the euphotic layer. Deck and *in situ* values are obtained by simulation using the model. The two curves are for the Equator and Arctic circle (t = 27 ° and 1°C respectively) and for the 21st March.

5.9. *Deck incubation vs* in situ *incubation methods*

The simulation of the "deck incubation method" (also called "simulated *in situ* method") is easily effected in a way similar to that used for the cloudiness effect. Clouds change the energy levels without modifying the spectral composition at each depth. Conversely, when samples from various depths are exposed on the deck using neutral filters to replicate the energy levels, the spectral composition of the incident radiation remains the same as daylight.

The model is therefore run with a modification which replaces the actual spectral distribution at each depth with that of daylight at the same instant, $E(0^+,\lambda,t)$. This replacement is achieved by constraining the integrals of both spectra to be equal (in terms of quanta). A deck experiment, with 100 "samples" (67 in the euphotic layer) incubated from sunrise to sunset, can thus be simulated, and the results compared with those obtained through the unmodified procedure (i.e. with an *in situ* experiment). The ratio $P_{deck}/P_{in\,situ}$ (both computed from 0 to Z_e) is shown in Fig.26 as a function of the chlorophyll concentration, for the vernal equinox at two latitudes (equator and arctic circle) and for two sea temperatures (27 and 1°C).

As expected, polychromatic daylight on the deck is more favourable than green submarine light which prevails in high-chlorophyll waters; P_{deck} is thus an overestimate (up to 20%) of the true production. The converse situation is observed in the case of blue, low-chlorophyll waters. The crossover at which the estimates agree, occurs for a chlorophyll concentration of about 0.5 mg m^{-3}. The difference between the two methods is, in principle, dependent on the spectral composition of the available radiation (i.e. on date and latitude). This dependence, however, is relatively weak especially when considering that rather extreme conditions have been selected for presentation in Fig. 26.

The deck incubation method has often been criticised, in particular because the underwater

spectral quality is not reproduced, or not easily reproducible. Surprisingly, the disagreement between *in situ* and simulated *in situ* methods is not as serious as might be suspected *a priori*, and perhaps the imperfect reproduction of the *in situ* temperature is a more crucial problem.

6. CONCLUSION

The physical factors are rather accurately parameterised in the present model, and if needed, improvements are easily accessible (particularly for the $\mathring{E}$-to-E_d ratio which could be made varying with depth). However, the physiological factors, whose role is crucial, remain inadequately documented and their parametrisation is debatable. This is particularly true for the yield and its irradiance dependence or for the temperature effect on growth. Therefore, it is not claimed that irrefutable data are produced when operating the model. Nevertheless, in its present state, it certainly provides clues for a better understanding of the interactive influences of the various environmental and biological factors. It provides quantitative explanations for the main features and tendencies of the primary production process in the global ocean and allows further sensitivity studies to be conducted.

While definitive estimates cannot be derived, the relative stability of the specific cross section for net photosynthesis, ψ^*, is very encouraging for future use at the scale made accessible by remote sensing techniques, especially when considering that the possible changes in ψ^* in response to seasonal, zonal and other environmental changes are also predictable. In addition, the ψ^* values, as produced by the model, confirm those already obtained in the field. This agreement supports the idea that there is internal coherence between the bulk properties measured at sea (the integrated primary production) and the physiological properties determined *in vitro* (such as the specific absorption or the quantum yield for growth). The model also allows some specific questions (the impact of inhibition, the effect of temperature, or the deep production, for instance) to be separately addressed without a full control of other influences. As such it is also a sub-model to be incorporated into more general, ecological or geochemical, models describing the algal biomass development.

7. ACKNOWLEDGEMENTS

The work was supported by Centre National de la Recherche Scientifique (UA 353) and by Centre National d'Etudes Spatiales (contract 88/1285). The author would like to express his particular appreciation to B. Gentili for his efficient help in programming, and to R.C. Smith for valuable criticism and suggestions.

8. REFERENCES

AUSTIN, R.W. (1974) The remote sensing of spectral radiance from below the ocean surface. In: *Optical Aspects of Oceanography*, edited by N.G. JERLOV and E.S. NIELSEN, 317-344, Academic, San Diego, California.

BAKER, K.S. and R. FROUIN (1987). Relation between photosynthetically available radiation and total insolation at the ocean surface under clear skies. *Limnology and Oceanography*, 32, 1370-1377.

BANNISTER, T.T. (1974) Production equations in terms of chlorophyll concentration, quantum yield, and upper limit to production. *Limnology and Oceanography*, 19, 1-12.

BANNISTER, T.T. and A.D. WEIDEMANN (1984) The maximum quantum yield of phytoplankton photosynthesis *in situ*. *Journal of Plankton Research*, 2, 275-294.

BERGER, W.H., K. FISHER, C. LAI and G. WU (1987) Ocean productivity and organic ocean flux. Part I. Overview and maps of primary production and export production. *Scripps Institution of Oceanography*, SIO ref. 87-30,

University of California.

BIDIGARE, R.R., R.C. SMITH, K.S. BAKER and J. MARRA (1987) Oceanic primary production estimates from measurements of spectral irradiance and pigment concentrations. *Global Biogeochemical Cycles*, **1**, 171-186.

BRICAUD, A., A MOREL and L. PRIEUR (1981) Absorption by dissolved organic matter of the sea (yellow substance) in the U.V. and visible domains. *Limnology and Oceanography*, **26**, 43-53.

CAMPBELL, J.W. and J.E. O'REILLY (1988) Role of satellites in estimating primary productivity on the northwest Atlantic continental shelf. *Continental Shelf Research*, **8**, 179-204.

COULSON, K.L. (1975) *Solar and terrestrial radiation*. Academic Press. 332pp.

DUBINSKY, Z., T. BERMAN and F. SCHANZ (1984) Field experiments for *in situ* measurement of photosynthetic efficiency and quantum yield. *Journal of Plankton Research*, **6**, 339-349.

EPPLEY, R.W. (1972) Temperature and phytoplankton growth in the sea. *Fisheries Bulletin*, **70**, 1063–1085.

FALKOWSKI, P.G. (1981) Light-shade adaptation and assimilation numbers. *Journal of Plankton Research*, **3**, 203-216.

GORDON, H.R. and A. MOREL (1983) Remote assessment of ocean color for satellite visible imagery. A review. *Lecture notes on Coastal and Estuarine Studies*, Springer-Verlag, New York, 114pp.

GROUPE MEDIPROD (1977) *Campagne GUIDOM 1976. Résultats des campagnes à la mer, n° 13.* Publications du CNEXO, 104pp.

HØJERSLEV, N.K. (1980) Water color and its relation to primary production. *Boundary-Layer Meteorology*, **18**, 203-220.

IKUSHIMA, I. (1967) Ecological studies on the productivity of aquatic plant communities. III. Effect of depth on daily photosynthesis in submerged macrophytes. *Botanical Magazine, Tokyo*, **80**, 57-67.

JAMART, B.M., D.F. WINTER, K. BANSE, G.C. ANDERSON and R.K. LAM (1977) A theoretical study of phytoplankton growth and nutrient distribution in the Pacific Ocean of the northwestern US coast. *Deep-Sea Research*, **24**, 753-773.

JERLOV, N.G. (1976) *Marine Optics*. Elsevier Oceanography Series, **14**, Elsevier, 231pp.

KIEFER, D.A. and B.G. MITCHELL (1983) A simple steady state description of phytoplankton growth based on absorption cross section and quantum efficiency. *Limnology and Oceanography*, **28**, 770-775.

KIRK, J.T.O. (1983) *Light and Photosynthesis in Aquatic Ecosystems*. Cambridge University Press, Cambridge, 401pp.

KIRK, J.T.O. (1984) Dependence of relationship between inherent and apparent optical properties of water on solar altitude. *Limnology and Oceanography*, **29**, 350-356.

LEE III, R.B., B.R. BARKSTROM and R.D. CESS (1987) Characteristics of the Earth Radiation Budget Experiment solar monitors. *Applied Optics*, **26**, 3090-3096.

LEWIS, M.R., R.E. WARNOCK, B. IRWIN and T. PLATT (1985) Measuring photosynthetic action spectra of natural phytoplankton populations. *Journal of Phycology*, **21**, 310-315.

LEWIS, M.R., N. KURING and C.S. YENTSH (1988) Global patterns of ocean transparency: implications for the new production of the open ocean. *Journal of Geophysical Research*, **93**, 6847-6856.

LIOU, K.N. (1980) *An Introduction to Atmospheric Radiation*. Academic Press , 392pp.

MALONE, T.C. (1976) Phytoplankton productivity in the apex of the New York Bight: environmental regulation of productivity-chlorophyll a. In: *The Middle Atlantic Continental Shelf and New York Bight*, M.G. GROSS, editor, Limnology and Oceanography Special Symposium, **2**, 260-272.

MALONE, T.C. (1987) Primary production of the ocean water column as a function of surface light intensity. *Deep-Sea Research*, **34**, 139.

MCCLATCHEY, R.A., R.W. FENN, J.E.A. SELBY, F.E. VOLZ and J.S. GARING (1971) Optical properties of the atmosphere, AFCRL-TR-71-0279, *Environment Research papers*, N°354.

MOREL, A. (1974) Optical properties of pure water and pure sea water, In: *Optical Aspects of Oceanography*, edited by N.G. JERLOV and E. STEEMAN NIELSEN, 1-24, Academic, San Diego, California.

MOREL, A. (1978) Available, usable, and stored radiant energy in relation to marine photosynthesis. *Deep-Sea Research*, **25**, 673-688.

MOREL, A. (1988) Optical modelling of the upper ocean in relation to its biogenous matter content (Case I waters). *Journal of Geophysical Research*, **93**, 10749-10768.

MOREL, A. and J.F. BERTHON (1989) Surface pigments, algal biomass profiles and potential production of the euphotic layer: relationships re-investigated in view of remote sensing applications. *Limnology and Oceanography*, **34**, 1545-1562.

MOREL, A. and L. PRIEUR (1977) Analysis of variations in ocean colour. *Limnology and Oceanography*, **22**, 709-722.

MOREL, A. and R.C. SMITH (1974) Relation between total quanta and total energy for aquatic photosynthesis. *Limnology and Oceanography*, **19**, 591-600.

MOREL, A., L. LAZZARA and J. GOSTAN (1987) Growth rate and quantum yield time response for a diatom to changing irradiances (energy and colour). *Limnology and Oceanography*, **32**, 1066-1084.

NECKEL, H. and D. LABS (1984) The solar radiation between 3300 and 12500 A. *Solar Physics*, **90**, 205-258.

NEUMANN, G. and W.J. PIERSON Jr. (1966) *Principles of Physical Oceanography*. Prentice-Hall Inc. 545pp.

PLATT, T. (1986) Primary production of the ocean water column as a function of surface light intensity: algorithms for remote sensing. *Deep-Sea Research*, **33**, 149-163.

PLATT, T., C.L. GALLEGOS and W.G. HARRISON (1980) Photoinhibition of photosynthesis in natural assemblages of marine phytoplankton. *Journal of Marine Research*, **38**, 687-701.

PLATT, T., S. SATHYENDRANATH, C.M. CAVERHILL and M.R. LEWIS (1988) Ocean primary production and available light: further algorithms for remote sensing. *Deep-Sea Research*, **35**, 855-879.

PRIEUR, L. and S. SATHYENDRANATH (1981) An optical classification of coastal and oceanic waters based on the specific spectral absorption curves of phytoplankton pigments, dissolved organic matter and other particulate materials. *Limnology and Oceanography*, **26**, 671-689.

PREISENDORFER, R.W. (1976) *Hydrologic Optics*, National Oceanic and Atmospheric Administration, Honolulu, Hawaii.

PREISENDORFER, R.W. and C.D. MOBLEY (1986) Albedos and glitter patterns of a wind-roughened sea surface. *Journal of Physical Oceanography*, **16**, 1293–1316.

SATHYENDRANATH, S., T. PLATT, C.M. CAVERHILL, R.E. WARNOCK and M.R. LEWIS (1989) Remote sensing of oceanic primary production: computations using a spectral model. *Deep-Sea Research* **36**, 431-453.

SIMONOT, J.Y. and H. LE TREUT (1986) A climatological field of mean optical properties of the world ocean. *Journal of Geophysical Research*, **91**, 6642-6646.

SPENCER, J.W. (1971) Fourier series representation of the position of the sun. *Search*, **2**, 172.

STEELE, J.H. (1962) Environmental control of photosynthesis in the sea. *Limnology and Oceanography*, **7**, 137-150.

STEEMAN-NIELSEN, E. and E.G. JORGENSEN (1968) The adaptation of plankton algae: I General Part. *Physiologia Plantarum*, **21**, 401-413.

TANRE, D., M. HERMAN, P.Y. DESCHAMPS and A. DE LEFFE (1979) Atmospheric modelling for space measurements of ground reflectances, including bidirectional properties. *Applied Optics*, **18**, 3587-3594.

TYLER, J.E. (1966) (Editor) Report on the second meeting of the Joint Group of experts on photosynthetic radiant energy. *UNESCO Technical Papers in Marine Science*, **2**, 1-11.

TYLER, J.E. (1973) (Editor) *Data report SCOR Discoverer expedition*. Scripps Institution of Oceanography. SIO Ref. 73-16.

WEBB, W.L., M. NEWTON and D. STARR (1974) Carbon dioxide exchange of *Alnus Rubra*: a mathematical model. *Ecologia*, **17**, 281-291.

WELSCHMEYER, N.A. and C.J. LORENZEN (1981) Chlorophyll-specific photosynthesis and quantum efficiency at subsaturating light intensities. *Journal of Phycology*, **17**, 283-293.

YENTSCH, C.S. (1974) Some aspects of the environmental physiology of marine phytoplankton: a second look. *Oceanography and Marine Biology, Annual Review*, **12**, 41-75.

YODER, J.A., L.P. ATKINSON, S.S. BISHOP, J.O. BLANTON, T.N. LEE and L.J. PIETRAFESA (1985) Phytoplankton dynamics within Gulf Stream intrusions on the southeastern United States continental shelf during summer 1981. *Continental Shelf Research*, **4**, 611–635.

APPENDIX 1

There are some recurrent problems in biological oceanography which originate from the ambiguous definition of PAR, the "Photosynthetic Available Radiation". No clear statement was made concerning the geometrical aspect of the radiative energy collection by aquatic plants. The SCOR Working Group 15 recommended a measurement of the "total (all visible wavelengths) downwelling irradiance", mainly because of "the technical problems associated with the measurement of scalar (spherical) irradiance" (TYLER, 1966). Some clarifications are needed.

As a result of the essentially planar character of the air-water interface, there is no doubt that the radiant flux able to enter a water body is exactly that which is measured on a horizontal surface just above the water, i.e. the downwelling irradiance $E_d(0^+)$. By integrating over the whole photosynthetic spectral range (λ_1 - λ_2 or generally 400-700 nm), PAR (0^+) in equation 1, for instance is thus

$$PAR\ (0^+)=\int_{\lambda 1}^{\lambda 2} (E_d(\lambda, 0^+)\ d\lambda$$

from which the flux just below the surface, at 0^-, can be computed as

$$PAR\ (0^-)=(1-r)\ PAR\ (0^+)$$

where r stands for the loss by external reflection at the interface. It is worth noting that if $E_d(\lambda, 0^+)$ or PAR (0^+) are accurately measured above the surface by using a flat and perfect cosine collector, PAR (0^-) cannot be, in practice, easily measured (at "null" depth) and, preferably, has to be computed.

In the underwater environment, the light field is spatially rearranged by scattering processes and internal reflection. Randomly oriented algal cells can collect radiations from all possible directions. Therefore PAR must definitely be defined as scalar irradiance, $\mathring{E}$, and measured by using a 4π -collector. This is also consistent with the fact that the amount of radiant energy absorbed per unit volume is expressed as the product $a.\mathring{E}$, where a is the absorption coefficient. It must be understood that PAR (Z) which appears in equations like 3, 4 or 5, for instance, is actually $\mathring{E}(Z)$.

Because of the double-faceted definition of PAR, a correct determination of the so-called light penetration profile would require, in principle, two instruments, one provided with a flat collector to obtain the "100%" level (alternatively measured above, at 0^+, or computed at 0^-, just below the interface) and another sensor, equipped with a spherical collector, to measure the available radiation within the water at various depths and, in particular, when determining the "1% level" referred to as the euphotic depth, Z_e. In the present paper, however, to conform to the most commonly accepted definition, Z_e keeps its conventional meaning, i.e. that depth where subsists 1% of the incident downwelling (quanta) irradiance.

The computations presented here rest on modelled downwelling irradiance profiles. It is, therefore, necessary to transform the E_d values into $\mathring{E}$ values in order to properly estimate the available radiation at all levels within the productive column and to compute the energy actually absorbed by algae. This is achieved by introducing a geometrical corrective term g (equal to the $\mathring{E}:E_d$ ratio and computed through equations 17 to 21). With g, in essence always greater than 1, and possibly reaching values of the order of 2, this "correction" is not trivial, but its importance has not been fully realized before. For instance MOREL (1978) wondered at embarrassingly high photosynthesis yield values obtained at the bottom of the euphotic layer, particularly at the values derived for eutrophic waters, where the predominantly green light is poorly absorbable by algae. In Appendix 2 of this paper the possibility is examined of having underestimated the actual available energy because E_d was used instead of $\mathring{E}$. The ratio $\mathring{E}:E_d$ was (wrongly) assumed to be less than 1.2, so this effect was judged insufficient to bring back the computed yields to within a more reasonable range. In the green ambience prevailing in eutrophic waters, however, with high scattering and relatively low absorption, the ratio $\mathring{E}:E_d$ can substantially exceed 1.2 (see curves for $\lambda = 570$nm in Fig. 4c). Therefore the problem raised by the inexplicably high quantum yield values is solved, or the "paradox" of high production in green waters, in effect, does not exist.

This geometrical effect which should be considered when computing the algal absorption has been acknowledged in a recent study (SATHYENDRANATH *et al.*, 1989). Their term "g" (using the above notation) is modelled as a linear combination of a first term, let equal to sec θ, for the direct sun light (with θ = zenith angle of the refracted sun rays) and for a second term for diffuse sky (let equal to 1.20). Such an approximation, which accounts for the directional character of the light penetrating the water (as in equation 14), incorrectly presumes that the geometrical structure of the incident light field is preserved within the entire water body without re-arrangements as a consequence of the scattering process.

APPENDIX 2

Under the assumptions (i), (ii) and (iii), the integration (equation 5) reduces to

$$P = 12\,\overline{Chl}\,\bar{a}^{*}\int_{0}^{L}\int_{0}^{Ze}\int_{\lambda 1}^{\lambda 2} PAR\,(Z, t)\,\varphi_{\mu}\,(\lambda, Z, t)\,d\lambda\,dZ\,dt$$

PAR being seen as a global polychromatic radiant flux, its λ-dependency drops out and this term can be separately integrated with respect to time and depth, according to

$$\int_{0}^{L}\int_{0}^{Ze} PAR\,(t, Z)\,dt\,dZ = \int_{0}^{L} PAR\,(0^{+}, t)\,dt \int_{0}^{Ze} \exp\,(-\bar{K}Z)\,dZ$$

Z_e is the depth of the euphotic layer, where the radiant flux falls to 1% of its surface value, so that $\exp\,(-\bar{K}Z_e) = 0.01$ and $\bar{K}Z_e = 4.6$. Therefore the above expression after integrating becomes

$$\overline{PAR}\,(0^{+})\,0.99/\bar{K} \simeq PAR\,(0^{+})\,Z_e/4.6$$

By noting that $\overline{Chl}\,.\,Z_e = \langle Chl\rangle_{TOT}$, the final equation 12 is found.

APPENDIX 3

By assuming a solar constant of 1368 W m^{-2} (LEE, BARKSTROM and CESS, 1987), the energy intercepted by our planet amounts to 174 PW. The mean planetary albedo and atmospheric absorptions result in only about 43% of this flux reaching the bottom of the atmosphere (see, e.g. LIOU, 1980), of which 80% reaches the ocean surface. After a loss by reflection (5%) this flux enters the ocean. About 45% of this radiant energy falls inside the photosynthetic band (see e.g.BAKER and FROUIN, 1987). The available energy (PAR) is therefore on average 26 PW.

In correspondence with a fixation of about 27 Pg C y^{-1} in the world ocean according to a recent study (BERGER, FISHER, LAI and WU, 1987), the photosynthetically stored energy, PSR, represents 0.033 PW. Therefore the PSR to PAR ratio is 1.27 10^{-3}. By reverting equation 1 where ψ^{*} is given the value 0.07m^2(g Chl)$^{-1}$, it follows that $\langle Chl\rangle_{TOT}$ = 0.018g Chl m^{-2}. With uniform vertical distribution this value corresponds to a mean chlorophyll concentration of 0.275 mg Chl m^{-3} (equation 30), associated with an euphotic depth of 66 m. Regarding their optical properties, such waters are between Jerlov's type IB and II (MOREL, 1988). By comparison with the regional distribution of optical water types given by JERLOV (1976) as well as with more detailed recent studies (SIMONOT and LE TREUT, 1986; LEWIS, KURING and YENTSCH, 1988) providing climatological fields of optical properties for the global ocean, such IB/II waters can well be seen as a representative "mean" oceanic water from optical and biological viewpoints.

The ambition of such a rough approach is not to produce irrefutable new figures, but just to point out the consistency within results from various fields (climatology, optics and biology) including the value of the index ψ^{*}. In sensitivity tests and other related studies, the model has been run with a Chlorophyll concentration of 0.3 mg m^{-3}, adopted as a typical mean oceanic value.